https://doi.org/10.1016/j.ymssp.2021.108512

On the leak-induced transient wave reflection and dominance analysis in water pipelines

Ying Zhang [1]; **Huan-Feng Duan** [2*]; **Alireza Keramat** [3]; **Tong-Chuan Che** [4]

[1] Ph.D. Candidate, Department of Civil and Environmental Engineering, The Hong Kong Polytechnic University, Hung Hom, Kowloon, Hong Kong SAR, PR China.

[2] Associate Professor, Department of Civil and Environmental Engineering, The Hong Kong Polytechnic University, Hung Hom, Kowloon, Hong Kong SAR, PR China.

[3] Research Assistant Professor, Department of Civil and Environmental Engineering, The Hong Kong Polytechnic University, Hung Hom, Kowloon, Hong Kong SAR, PR China.

[4] Postdoctoral Research Associate, Department of Civil and Environmental Engineering, The Hong Kong University of Science and Technology, Clear Water Bay, Kowloon, Hong Kong SAR, PR China

[*]*Corresponding Author, E-mail: hf.duan@polyu.edu.hk*

Abstract

The leak-induced reflection information forms the basis of developing and applying transient-based leak detection methods in water-filled pipelines. The transient reflection method (TRM) has been widely incorporated in various leakage problems, and affecting parameters in the process are closely investigated in specific cases. However, the TRM literature lacks a global assessment of the relative importance of each parameter for a general inference on the contribution of each independent variable to the desired reflection criterion, which assists in leakage management. Besides, in the majority of previous studies, the leak-induced reflection wave at the measurement point is approximated by that at the leaky point, i.e., the propagation behavior and process of the reflected wave from the potential leak location to measurement point is ignored, leading to inaccuracy in sizing potential leaks by the TRM. To resolve these issues, this study firstly derives the leak-induced reflection coefficient at the measurement point by incorporating the additional damping effect of the reflection wave propagation process along the pipeline, which is then fully validated by MOC-based numerical and experimental laboratory applications. To further understand the contribution of different factors in the derived reflection coefficient, a systematic analysis is conducted based on dimensional analysis and extensive numerical simulations. The obtained results are characterized by the dominance analysis so as to explore the importance ranking of different dimensionless factors to the leak-induced reflection coefficient in the pipeline system. The analysis results indicate that, amongst all the dimensionless parameters, the leak factor provides the largest influence and contribution to the wave reflection coefficient (with about 40% contribution), followed by the transient intensity (23%) and initial system and flow conditions (20%), and lastly the measurement distance from leak location (17%). The finding of this study is helpful in leakage management as it aims to understand and explain the applicability and

effectiveness of the TRM under different conditions.

Keywords: pipeline health monitoring; leak detection; wave reflection; transient reflection method (TRM); wave signal processing; dominance analysis

1. Introduction

According to the World Economic Forum Report, the water crisis ranks top five among the top global risks in the recent five years, especially in 2015. The considerable quantity of water leakage, which often occurs due to pipe aging and corrosion in water supply distribution networks, intensifies the severity of water scarcity and endangers the security of drinking water. Specifically, the negative pressures induced by rarefaction water hammer waves cause intrusion of external contaminants through the leaky points, which in turn leads to water quality loss and/or sedimentation and blockage [1-3]. According to World Bank data, the non-revenue water rates in developing nations are at least 35% and even as high as 50% in some water supply systems. Surprisingly, in some developed countries, such as Italy, water loss levels also suffer a pretty high rate of 70% due to the aging of the pipe systems [4].

Therefore, timely leakage detection is of great importance to the daily operation and periodical maintenance of urban water supply pipelines (UWSP). Passive acoustic techniques are the most commonly used approach by the water authority since fluid jetting from a small orifice generates high-frequency oscillations in the pipe wall. Consequently, listening devices can be used at the first stages to estimate the leak location by moving the device along the pipe until leak-induced maximum noise is detected [5]. However, the main limitations of this method are: (1) only applied to short-distance range as leak-induced noise attenuates rapidly about 250 m [6]; (2) low tolerance to background noise [6, 7]. The transient-based methods (TBMs) have received increasing attention in detecting pipes' defects in recent years to tackle the problems mentioned

above in passive acoustic techniques [3, 8-22]. In addition, high efficiency, low cost, and non-intrusive characteristics are the advantages of TBMs compared with other leakage detection methods.

Transient flow is often caused by instantaneous/sudden flow rate change from one steady-state to another steady-state. This sudden velocity change invokes a sharp pressure variation that propagates along the pipe in axial and radial directions [23]. Transient waves are actively injected at accessible points (e.g., fire hydrants or valves) into the water supply pipes through which they propagate and interact with the pipelines' physical discontinuities or boundaries [12, 15, 16, 24, 25]. Thus, the measured transient waves are rich in pipe configuration information, capable of detecting faults in pipes. For example, in the time domain, a leak, as one type of physical discontinuities in the pipe, not only induces the exponential damping of the transient pressure peaks [15, 26-28] but also produces additional reflection signals with opposite sign of the incident pressure wave [16, 17, 29] compared with the transient signal of the corresponding intact pipe. In detail, the characterization of the transient signal is distinguished by leak size, shape, location, discharge condition, and the pressure at the leak [17]. The relative importance of the damping effects of a leak in water pipelines has been investigated, revealing that all transient-based leak detection methods can not accurately detect the leak if the leak-induced reflection is neglected [14]. In the frequency domain, a leak modifies the amplitude of the transient signal's resonant peaks for both the single uniform pipeline [18, 22, 30] and complex pipelines [19, 20], which can be applied to locate and size leaks by extracting the pattern of leak-induced harmonic peaks.

Among all the other transient-based leak detection methods, the transient reflection-based method (TRM) is the easiest to understand and apply [1]. The tenet of this method is summarized as follows: the distance between the leak and the measurement point is estimated by $d = a\delta t / 2$,

where δt is the traveling time or time lag between the instant at which the incident wave arrives at the measurement point and the instant at which the first reflected wave from the leak reaches the measurement station. Once δt is measured, *d* is determined for a given wave-speed *a*. Several signal processing techniques have been developed to improve the identification of leak-induced reflection time. Pan, et al. [31], Taghvaei, et al. [32], and Shucksmith, et al. [33] developed the Cepstrum method to enhance identifying the time lag. Nguyen, et al. [34] compared the proposed least-squares deconvolution approach to the Cepstrum method for impulse response function (IRF) estimation for leak localization in a reservoir-pipeline-valve (RPV) system, finding a satisfactory suppression of the artefacts in the IRF. Ferrante [35, 36] applied wavelet analysis of numerical and experimental pressure signals with noise to leak positioning based on the fact that the discontinuity of the pipe induces the singularity of transient pressure signal in the time domain which performs as local maxima in the wavelet transform modulus. Liou [37], Lee, et al. [18] and Beck, et al. [38] introduced the cross-correlation method to improve the sharpness of the reflected leak signal to pinpoint the leak. Lee, et al. [39] developed a cumulative sum change algorithm to detect the leak location based on the measured experimental transient trace and numerical modeling result of the corresponding intact pipe. Time-frequency domain techniques based on empirical mode decomposition have been used for extracting leak reflection features [40]. Besides, the artificial neural network technique has also been applied for leak location detection in a liquefied gas pipeline using training data generated by the transient numerical model [41]. All these leakage identification techniques can provide insight into the significance of parameters involved in the process for a given set of system properties. The literature on leakage management lacks a global analysis to rank the importance of variables (predictors) in predicting the criterion (the leak reflection), which is a helpful result in evaluating and characterizing the transient-based leak

detection methods. This study adopts a robust technique to rank the relative importance of the critical parameters involved in the detection process. The preceding studies only investigated specific factors that influence leak detectability through leak-reflection signals [65, 72]. In contrast, this study seeks to examine their relative importance, in general. To this end, an explicit expression for the criterion (the leak reflection) is derived which is used to generate samples for the global parameter importance analysis.

An established technique in the multiple regression theory called the dominance analysis (DA) is incorporated to rank the influential components. The DA offers a robust global measure for variable importance in multivariate regression. Based on the practical perceptions, four dimensionless variables are identified as the main predictors of the leak reflections. Then, their relative importance is evaluated considering an analytically derived formula for the dependent variable (the criterion). As a global measure, DA treats all involved predictors as random variables, thus determining one predictor's dominance over others by comparing their additional contributions across all subset models. It does not need any derivative information, but only the sample matrix and the corresponding model output values are required [42-44]. As for sizing the leak, Jönsson and Larson [29] analytically derived the magnitude of leak-induced reflected wave at the leakage point in a frictionless pipe section by solving wave equations. Brunone and Ferrante [17] obtained the semiempirical relation between measured leak-induced reflection coefficient and leak-related dimensionless damage based on the optimization analysis of experimental data and numerical model under the frictionless assumption. Covas, et al. [45] transformed the formula developed by Jönsson and Larson [29] to preliminarily estimate leak rate by using the magnitude of leak-induced reflection wave, initial transient wave at one measurement point, and steady-state pressure head at leak as it neglects the friction losses in their pipe systems. Capponi, et al. [46]

emphasized the non-uniqueness of the leak information (leak size and initial steady-state pressure head at the leak) for a certain measured leak-induced reflection coefficient. Wang, et al. [47] estimated the size of leaks by leak-induced reflection wave in water pipelines using transients considering quasi-steady friction-induced wave attenuation. Although the previously mentioned TRMs have demonstrated their applicability for a rough estimation of leak size, they either consider a frictionless case or use a weak steady friction assumption. In other words, the leak-induced reflection amplitude at the measurement point is assumed equivalent to that of the leak point. In real practice, the reflection wave at the leak point attenuates during the propagation from the leak to the measurement point, so to apply the measured reflections to size the leak, a more accurate evaluation is required, which is among the aims of this study.

Several TBMs of leak detection have been offered in the literature as addressed, which usually have errors beyond the theoretical expectations in actual practice. However, they fail to address this drawback adequately and do not rank the contribution of different predictors toward an accurate leakage identification and management in the TRM. A significant cause for this inaccuracy associates with incomplete knowledge about the magnitude of the reflected wave from a leak which is essentially a function of (i) leak size and location, (ii) system parameters as well as initial conditions, and (iii) the injected transient wave. To fill this knowledge gap, this paper derives an analytical formula for the dependent variable (the leak reflection criterion) and employs it to rank the contribution of four dimensionless variables systematically using DA. The case of an unbounded system is considered in the analysis process as it eliminates the interference from boundaries in the localization management and isolates the main “pipe” and “fluid” parameters, thus allowing general conclusions on a global relative importance investigation.

This paper firstly derives an analytical formula for the leak-induced reflection coefficient at

the measurement point based on wave propagation theory by considering the quasi-steady friction. Then the results are validated by numerical experiments based on the method of characteristics (MOC) and the laboratory experiment from the literature. Finally, the dominance analysis is conducted to consider the relative importance of factors that influence the reflection coefficient, thus giving some insights to leak detection.

2. Methodology

This section essentially describes the transient wave propagation in the presence of a leak in a pipeline and presents a brief introduction about the dominance analysis to evaluate the relative importance of the model's practical components.

2.1 Essentials of the wave theory

2.1.1 Leak-induced reflection coefficient

The simplified one-dimensional (1D) water hammer model [48] is composed of the continuity and momentum conservation equations, as expressed in Eq. (1) and (2), respectively:

$$\frac{gA}{a^2}\frac{\partial H}{\partial t}+\frac{\partial Q}{\partial x}=0 \tag{1}$$

$$\frac{1}{gA}\frac{\partial Q}{\partial t}+\frac{\partial H}{\partial x}+\frac{f_D Q^n}{2gDA^n}=0 \tag{2}$$

in which H = instantaneous pressure head in time; Q = instantaneous discharge in time; A = pipe cross-sectional area of the pipe; D = pipe diameter; f_D = Darcy-Weisbach friction factor; n = exponent of velocity in the friction-loss term (n = 2 in this study); a = wave speed; t = time; x = spatial coordinate along the pipeline; g = gravitational acceleration. This equation set is based on the following assumptions: (1) the pipe wall's material is assumed to be rigid; (2) the system is free of cavitation (such as column separation and air pockets), leakages, blockages, and fluid-

structure interaction are assumed to be absent; (3) transient perturbation is assumed to be small so that governing equations can be linearized; (4) transient disturbance/operation is assumed to be fast enough to ensure not being disturbed by adjacent reflection source.

In steady-oscillatory flow, instantaneous pressure head H and instantaneous discharge Q can be characterized as the summation of the time-invariant mean value H_0, Q_0, and a deviation from the mean value: $H = H_0 + h^*$, $Q = Q_0 + q^*$. Since mean flow Q_0 and mean pressure head H_0 are time-invariant ($\partial Q_0/\partial t = 0$, $\partial H_0/\partial t = 0$) and Q_0 remains constant along the pipe ($\partial Q_0/\partial x = 0$), hence, the partial derivative terms in Eqs. (1) and (2) are simplified as

$$\frac{\partial Q}{\partial x} = \frac{\partial q^*}{\partial x} \qquad \frac{\partial Q}{\partial t} = \frac{\partial q^*}{\partial t} \tag{3}$$

$$\frac{\partial H}{\partial x} = \frac{\partial H_0}{\partial x} + \frac{\partial h^*}{\partial x} \qquad \frac{\partial H}{\partial t} = \frac{\partial h^*}{\partial t} \tag{4}$$

where $\frac{\partial H_0}{\partial x} = -\frac{f_D Q_0^2}{2gDA^2}$ for turbulent flow and $\frac{\partial H_0}{\partial x} = -\frac{-32\nu Q_0}{gAD^2}$ for laminar flow.

As illustrated in Figure 1 and Appendix A, the pressure and flow rate change at the leak after the transmission of the approaching transient pressure wave F_1. For the approaching and reflected waves, one can write

$$H_A - H_{A0} = F_1 + f_1 \tag{5-a}$$

$$Q_A - Q_{A0} = \frac{1}{k'}(F_1 - f_1) \tag{5-b}$$

where f_1 is the leak-induced reflected wave, H_A and Q_A are the pressure head and flow rate at the point after the incident wave passing through the leak, H_{A0} and Q_{A0} are the pressure head and flow rate at a point before the incident wave passing through the leak (i.e., steady-state), k' is wavenumber (i.e., Eq. (A.12) in Appendix A). The detailed derivation of these relations is explained in the Appendix A of this paper.

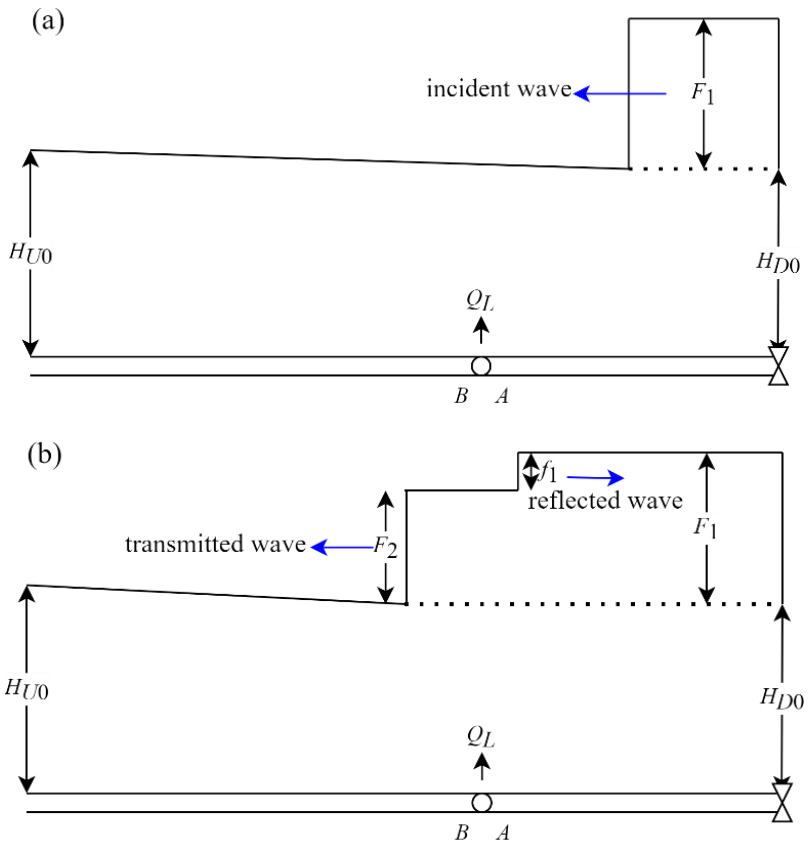

Figure 1 Sketches of transient pressure waves: (a) incident wave; (b) reflected waves from a leak.

Let points *A* and *B* in Figure 1 denote the virtual vicinal downstream and upstream of the leaky point. The transmission of F_1 is represented by F_2, so the pressure and flow rate variation at point *B* are:

$$H_B - H_{B0} = F_2 \tag{5-c}$$

$$Q_B - Q_{B0} = \frac{1}{k'} F_2 \tag{5-d}$$

where H_B and Q_B are the pressure head and flow rate at point *B* after the transmitted wave F_2 passes through the leak, H_{B0} and Q_{B0} is the pressure head and flow rate at point B before the incident wave arrives at the leak (i.e, steady-state).

The mass conservation in the case of the same pipe diameter at either side of the leak allows

for

$$Q_A - Q_B = Q_L \Rightarrow V_A - V_B = \frac{Q_L}{A} \tag{5-e}$$

$$Q_{A0} - Q_{B0} = Q_{L0} \Rightarrow V_{A0} - V_{B0} = \frac{Q_{L0}}{A} \tag{5-f}$$

where Q_L is the magnitude of the leak discharge through the orifice, V is the mean velocity of cross-section, which is defined by the ratio of the flow rate to the cross-sectional area, subscripts A and B indicate the neighboring upstream and downstream of the leak. Omitting the pressure head loss at the leak point gives

$$H_B = H_A = H_L \tag{5-g}$$

$$H_{B0} = H_{A0} = H_{L0} \tag{5-h}$$

The leak is modeled by the orifice (or Torricelli's) equation where the fluid is discharged into the air as follows

$$Q_L = C_d A_L \sqrt{2gH_L} \tag{5-i}$$

$$Q_{L0} = C_d A_L \sqrt{2gH_{L0}} \tag{5-j}$$

where H_L = pressure head at leak, C_d = discharge coefficient, A_L= leak area.

By combining the Eqs. (5-a) ~ (5-j), the reflected wave f_1 at the leak point is expressed as

$$f_1 = -\frac{k'}{2}\left(Q_L - Q_{L0}\right) = -\frac{k'}{2} C_d A_L \sqrt{2g}\left(\sqrt{H_{L0} + F_1 + f_1} - \sqrt{H_{L0}}\right) \tag{6}$$

which can be rearranged to a quadratic function for the unknown f_1. The solution of Eq. (6) is

$$f_1 = \frac{1}{8}\frac{k'^2\alpha^2 Q^2_{S0}}{H_{L0}} + \frac{k'}{2}\alpha\left|Q_{S0}\right| - \frac{1}{2}\frac{k'}{2}\frac{\alpha\left|Q_{S0}\right|}{\sqrt{H_{L0}}}\sqrt{\left(\frac{k'}{2}\frac{\alpha Q_{S0}}{\sqrt{H_{L0}}}\right)^2 + 4\left(\frac{k'}{2}\alpha\left|Q_{S0}\right| + H_{L0} + F_1\right)} \tag{7}$$

where $\alpha = Q_{L0}/Q_{S0}$ = leakage factor, Q_{S0} is the steady-state flow rate at the upstream point of the leak. From this equation, it is straightforward that f_1 theoretically relates to leakage character (leakage factor α and the steady-state local pressure at leak H_{L0}), initial condition Q_{S0}, incident transient pressure wave F_1 and wave number k'. To quantify the leak-induced reflection coefficient

at the leak, the criterion C_{ref_L} is defined as the ratio between the amplitude of the reflected wave and the incident wave:

$$C_{ref\_L} = \frac{|f_1|}{|F_1|} \tag{8}$$

Particularly, for a frictionless pipe, if the transient is generated by a sudden full closure of the downstream valve (the corresponding *Joukowsky* head ΔH_{jou} equates to the incident wave F_1 at the leak), one can obtain the reflection coefficient without frictional effects $C_{ref\_L}^{FL}$ as follows (with details shown in Appendix B):

$$C_{ref\_L}^{FL} = 2\delta^2\chi + 2\delta - 2\delta\sqrt{(\delta\chi+1)^2+\chi} \tag{9}$$

where $\chi = \frac{F_1}{H_{L0}}$, $\delta = \frac{\alpha}{4(1-\alpha)}$, and superscript "*FL*" represents frictionless case.

In fact, this result is identical to the derived leak-induced reflection coefficient by Jönsson and Larson [29] or its inverse function [45], which can be used to estimate the leakage factor α by measuring F_1 and f_1 for an approximate H_{L0}.

2.1.2 Pressure wave damping along the pipeline

For a physically continuous pipe section, the propagation of pressure oscillation can be represented as:

$$h^*(x,t) = h^{tr} e^{-j\mu x} e^{jwt} = h^{tr} e^{\mu_j x} e^{j(wt-\mu_r x)} \tag{10}$$

where h^{tr} is the transmitted wave. Hence, the pressure oscillation amplitude with space can be obtained as,

$$h_{amp} = \left|h^{tr}\right| e^{\mu_j x} \tag{11}$$

where x is the distance that the pressure wave has traveled, μ_j describes the frequency-dependent attenuation by friction effects along the pipe, and the absolute value symbol represents the

magnitude of the holding complex number. This equation shows that the amplitude of the pressure wave exponentially dampens with the distance as it travels.

Assuming that transient is generated by the downstream valve ($x = 0$),

$$\left(h_{amp}\right)_{DV} = \left|h^{tr}\right| \tag{12}$$

and propagating toward the leak location, the amplitude of this incident wave at point A (downstream of the leak) is

$$\left(h_{amp}\right)_{A} = \left|h^{tr}\right| e^{\mu_j y_L} \tag{13}$$

where y_L indicates the distance from the transient source to the leak point. As a result, at the leak ($y = y_L$), the reflected wave amplitude is

$$\left(h_{amp}\right)'_{A} = \left(h_{amp}\right)_{A} C_{ref\_L} \tag{14}$$

The reflection again attenuates as it propagates from point A to the measurement point ($y = y_M$)

$$\left(h_{amp}\right)'_{M} = \left(h_{amp}\right)'_{A} e^{\mu_j d} \tag{15}$$

where d indicates the distance between the leak and the measurement point.

2.1.3 Reflection coefficient at the measurement point

Considering Eqs. (12)-(15), the amount of attenuation during the wave travel is achievable. The desired ratio of the reflected amplitude to the incident wave at the measurement point is

$$C_{ref\_M} = \frac{\left(h_{amp}\right)'_{M}}{\left(h_{amp}\right)_{M}} = \frac{C_{ref\_L}\left|h^{tr}\right| e^{\mu_j y_M} e^{\mu_j d} e^{\mu_j d}}{\left|h^{tr}\right| e^{\mu_j y_M}} = C_{ref\_L} e^{\mu_j (2d)} \tag{16}$$

The analytical solution in Eq. (16) indicates that the reflection coefficient at the measurement point depends not only on the reflection coefficient at the leak but also on the distance between the leak and measurement location d, friction factor f_D, and the frequency w. Similar derivation procedure can be applied to the case of total friction effect (i.e., steady friction and unsteady friction) and the

key results are obtained and shown in Appendix C. More discussion about the impacts of unsteady friction is given in following numerical applications in this study.

2.2 Dominance analysis

In behavioral, statistical science, and social psychology, researchers often select multiple regression to explain the response (criterion) variable (Y) and predictors (X_1, X_2, …, X_N). Numerous indexes, such as standardized regression coefficient, structure coefficients, relative weights as well as goodness-of-fit R or R^2 can be used as measures of the model predictors' relative importance in multiple regression [42, 43, 49]. The relative importance not only indicates the most dominant predictor among all independent variables, but also implies the importance ranking of the remaining factors after controlling some predictors.

The dominance analysis (DA) proposed by Azen and Budescu [44], based on the calculation of R^2 for all subset models, is chosen as the indicator for intuitive importance interpretation in this paper. The adopted DA technique offers a robust global measure for variable importance in multiple regression. As a global measure, DA determines one predictor's dominance over others by comparing their additional R^2 (or pseudo-R^2) contributions across all subset models. It does not need any derivative information, but only the sample matrix and the corresponding model output values are required. DA is one of the more powerful principles in decision theory which has the following distinct capabilities [42]: (a) allows for making decisions to select a few predictors rather than the full ranking, (b) explicitly acknowledge the extent that one predictor dominates the dependent variable, (c) is quite general that can accommodate various measures.

For clarity, the framework and application procedure of the developed DA, as well as the model results, are demonstrated as in Figure 2.

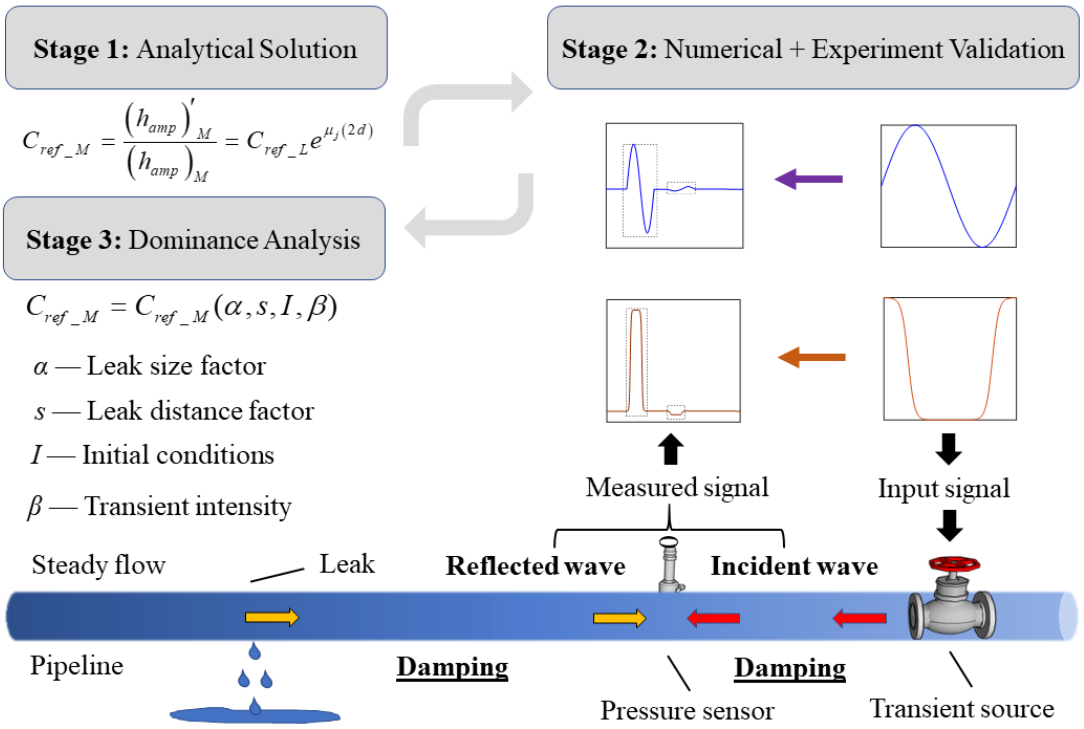

Figure 2 Framework of the method development and application procedures

This study firstly derives the analytical leak-induced reflection coefficient at the measurement station by incorporating the additional damping effect of the reflection wave propagation process along the pipeline. Next, the accuracy of this analytical solution is validated by MOC-based numerical experiments considering two different signals and experimental laboratory applications. A systematic analysis is then conducted based on dimensional analysis and extensive numerical simulations to infer the contribution of various factors on the derived reflection coefficient. The DA characterizes the ranking of different dimensionless factors to the leak-induced reflection coefficient pipeline systems in general.

3. Validation and Analysis of Analytical Results

3.1 Comparison with MOC results

To validate the analytical solution derived in Eq. (16), firstly, two numerical unbounded pipe-valve

systems with one leak (shown in Figure 3) are considered for precise observation of incident wave and reflected wave. The pressure head H_{U0} and flow rate Q_{S0} at pipe upstream are set as 40 m and 0.015 m^3/s, respectively, which remain constant to simulate non-reflective upstream boundary. The corresponding system parameters for two numerical experiments are listed in Table 1. Leak location and measurement location is normalized by pipe length L, i.e., $y_L^* = y_L/L$, $y_M^* = y_M/L$. Transient is generated by different perturbation operations on the downstream valve (DV): (i) single-frequency sinusoidal oscillation for numerical test Case 1, and (ii) sigmoid-shaped impulse oscillation for numerical test Case 2. After the valve perturbation duration T_v, the DV opening returns to its original state.

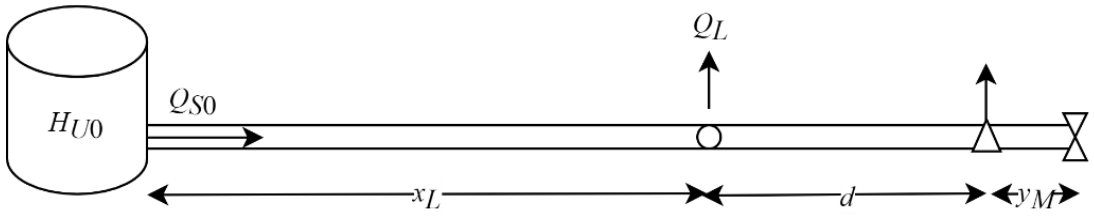

Figure 3 The pipeline system with one leak for the numerical investigation

Table 1 System information for numerical tests

Case No.	L (m)	D (m)	f_D	a (m/s)	Q_{S0} (m^3/s)	y_L^*	α	y_M^*	Input Signal Type	I
1	5000	0.2	0.015	1000	0.015	0.6	0.15	0.3	sinusoidal perturbation	0.1791
2	5000	0.2	0.015	1000	0.015	0.6	0.3	0.3	sigmoid-shaped pulse	0.1791

Duan, et al. [50] proposed a lumped dimensionless system parameter $I = f_D ML/D$ to evaluate the relative importance of unsteady friction damping to the total friction damping γ_{fitted} during transients, where $M = V/a$ is the *Mach* number. They concluded that unsteady friction plays a less

important role in larger pipe scale (L/D) and higher M or Reynolds numbers compared to quasi-steady friction. Meniconi, et al. [51] further validated this work by extending the range of Reynolds number from smooth to rough pipe-flows by comparing laboratory data and field data with numerical pressure signals simulated by a one-dimensional (1D) water hammer model when only quasi-steady friction term is considered. The larger value of γ_{fitted} means the more importance of unsteady friction-induced damping to the total friction damping. According to his fitted result, it has

$$\gamma_{\text{fitted}} = 1.8\times10^{-1}\text{e}^{-4.85I} \text{ for } 10^{-2} \le I \le 1.0 \tag{17}$$

According to Duan, et al. [50], the contribution of the unsteady friction to total damping is 7.6% for these two cases, so ignorance of the unsteady friction term in the numerical solution is acceptable in both cases. This result can also be evidenced by the analytical results and numerical tests (e.g., Table C1, Figures C1 and C2) in Appendix C.

The 1D water hammer model with quasi-steady friction (Eqs. (1) and (2)) is numerically solved by the method of characteristics (MOC) [48]. The spatial step Δx and time step Δt are set as 0.1 m and 0.0001 s, respectively, to satisfy the Courant condition for wave speed a = 1000 m/s. The measurement point y_M^* = 0.3 locating between the leak and the DV is taken in the analysis.

3.1.1 Numerical Case 1

At the steady state, the pressure head for DV (y = 0) is H_0 = 36.37 m. The pressure head oscillates at DV with a single angular frequency for a time duration T_v = 2 s. After T_v, the DV returns to its original opening, so the following expressions represent the variations of the injected pressure head with time:

$$H = \begin{cases} H_0 + H_0 \sin(w_{in}t); & \text{when } 0 < t < T_v; \\ H_0; & \text{when } t > T_v. \end{cases} \tag{18}$$

Hence, the generated transient pressure wave amplitude $(h_{amp})_{DV}$ equates to H_0 = 36.37 m.

The numerical transient pressure response at $y_M = 0.3L$ is shown in Figure 4(a). As shown in this figure, the sinusoidal-shaped transient pressure wave generated by the DV firstly arrives at the measurement point at $t_1 = y_M/a$ =1.5 s and after $T_v/4$ = 0.5 s, its amplitude $(h_{amp})_M$ reaches the peak (73.22–37.31 = 35.9 m), so that $(h_{amp})_M = (h_{amp})_{DV} e^{\mu_j d} = 36.37 \times 0.9775 = 35.55$ m is obtained through Eq. (16). The error between numerical and predicted pressure head amplitude is 1.0%, thus validating the derived friction-induced damping of the transient pressure wave. Then this incident wave encounters the leak point and reflects with an opposite sign and arrives at the measurement point at $t_3 = t_1 + 2d/a$ = 4.5 s.

The incident wave $h_{in}^* = H_{in}(t) - H_0$ ($t_1 < t < t_2$), and the reflected wave $h_{ref}^* = H_{ref}(t) - H_0$($t_3 < t < t_4$) can be extracted from the measured pressure trace by applying a rectangular time window. By applying Fast Fourier Transform (FFT) algorithm to these two waves of identical frequency, the discrete numerical signals in the time domain are transformed into the frequency domain and then nondimensionalized by the incident wave's maximum power, as seen in Figure 4(b). It is noted that the incident wave must end before the arrival of the leak-induced reflection wave at the measurement point, therefore $T_v < 2d/a$. The period of the input sinusoidal signal should not be more than T_v (i.e., $2\pi/w_{in} < T_v$), hence, the selected angular frequency w_{in} of the input signal should be larger than $\pi a/d$ (i.e., $w_{in} > \pi a/d$). Accordingly, a dimensionless frequency w^* is introduced as follows: $w^* = w_{in}/w_e$, $w_e = \pi a/d$, which describes the effective frequency for an unbounded piping system. Thus, a larger value of w^* means the higher frequency of the incident wave.

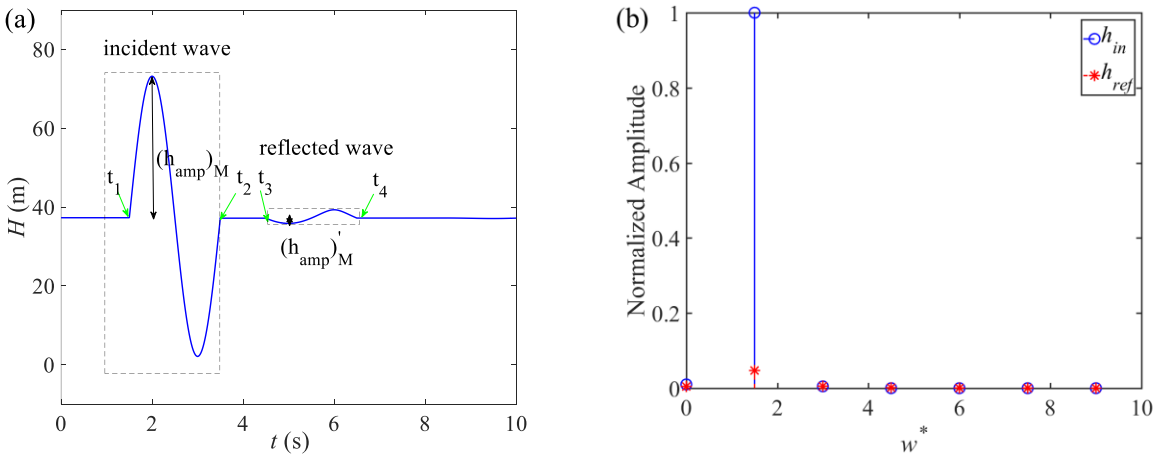

Figure 4 (a) Pressure trace at the measurement location (y_M^*=0.3), (b) the normalized frequency spectrum of the incident and reflected waves for Case 1 (w_{in}^*=1.5)

Table 2 Numerical validation of derived leak-induced reflection coefficient (Case 1, w_{in}^*=1.5)

	Predicted value (Analytical)	MOC result (Numerical)	Error (%)
$(h_{amp})_M$ (m)	35.55	35.91	1.0
$(h_{amp})'_M$ (m)	1.32	1.32	0.0
C_{ref_M} (%)	3.71	3.68	0.7

Figure 4(b) shows that the incident wave and reflected wave at the measurement point have the same frequency. Hence, we can directly obtain the leak-induced reflection coefficient for this input frequency by dividing $(h_{amp})'_M = 37.20 - 35.88 = 1.32$ m by $(h_{amp})_M$ obtained from the numerical pressure trace at the measurement point, as illustrated in Table 2.

For Case 1, a series of the single low and high sinusoidal oscillations at DV have been conducted and followed by the steps described previously to obtain the $\tilde{C}_{ref\_M}$ corresponding to the given incident frequency. Figure 5(a) shows the MOC-based numerical and analytical

reflection coefficients are in the defined frequency range $w^* \sim (1,1000)$. The two sets of results are in good agreement, which can further be explained by the frequency-dependent term k' in Eq. (A.12). Substitute the expression of μ and R for turbulent flow into k', there is

$$k' = \frac{a}{gA}\sqrt{1 - j\frac{f_D Q_0}{DAw}}, \quad \frac{f_D Q_0}{DAw} = \frac{f_D V_0}{Dw^* w_e} = \frac{f_D}{w^*\pi}\frac{V_0}{a}\frac{d}{D} = \frac{f_D M}{w^*\pi}\frac{0.3L}{D} \tag{19}$$

where $M = V_0/a$ = Mach number. In this case, $\frac{f_D M}{w^*\pi}\frac{0.3L}{D} \approx \frac{0.0171}{w^*} \in (10^{-5}, 10^{-2}) << 1$. As a result, $k' \approx a/(gA)$ which indicates that k' is approximately independent of the frequency.

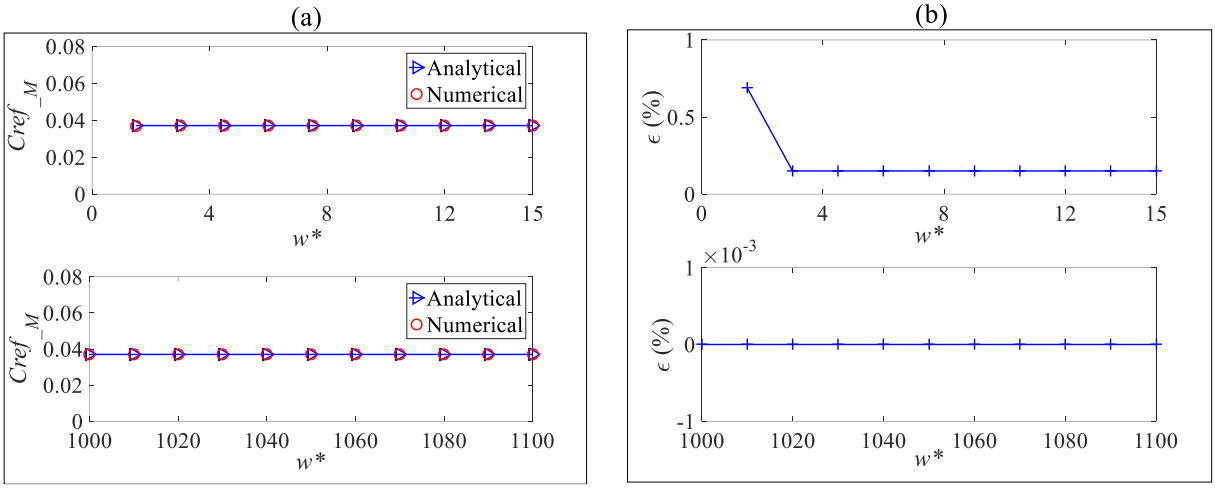

Figure 5 Numerical results for Case 1: (a) leak-induced reflection coefficient for different frequency domains; (b) relative error of analytical results

For evaluation, the relative difference (error) between the numerical value indicated by $\tilde{C}_{ref\_M}$ and analytical value (C_{ref_M}) is adopted:

$$\varepsilon(\%) = \left|\frac{C_{ref\_M} - \tilde{C}_{ref\_M}}{C_{ref\_M}}\right| \times 100 \tag{20}$$

This error $\varepsilon < 0.7\%$ in Figure 5(b) validates the accuracy of the analytical results.

3.1.2 Numerical Case 2

For this case, the flow oscillation imposed on the DV is

$$Q=\begin{cases} Q_0\left(1-\dfrac{1}{1+\mathrm{e}^{(-c_1)*(t-c_2)}}\right); & \text{when } t<T_v/2; \\ Q_0\left(1-\dfrac{1}{1+\mathrm{e}^{(-c_1)*(T_v-t-c_2)}}\right); & \text{when } t>T_v/2. \end{cases} \tag{21}$$

For a comparative analysis, three sigmoid-shaped impulse oscillations with different T_v (as shown in Table 3) are considered to cover a wide range of signal bandwidths. The measured transient pressure responses for Cases 2A~2C are shown in Figure 6(a). As shown in this figure, taking Case 2A as an example to illustrate, the sigmoid-shaped impulse transient pressure wave generated by the DV with T_v = 2 s firstly arrives at the measurement point at $t_1 = y_M/a$ = 1.5 s and finishes at $t_2 = t_1+T_v$ = 3.5 s. Then this incident wave encounters the leak point and reflects back at $t = y_L/a = t_1+d/a$ = 3 s with opposite sign and later arrives the measurement point at $t_3 = t_1+2d/a$ = 4.5 s. The incident wave $h_{in}^* = H_{in}(t) - H_0$ (with $t_1 < t < t_2$), and the reflected wave $h_{ref}^* = H_{ref}(t) - H_0$ (with $t_3 < t < t_4$) can be extracted from the measured pressure trace by applying a rectangular time window. By applying Fast Fourier Transform (FFT) to these two wave signals, the discrete numerical signals in the time domain are transformed into the frequency domain. Then they are nondimensionalized by the incident wave's maximum power (see Figure 6(b)). The frequency spectrum of the sigmoid-shaped impulse excitation has the Sinc function features, i.e., 50% of the full lobe bandwidth falls in $w^* \in$ (0, 1.5) [52], and 90% of it falls in $w^* \in$ (0, 2.7) in this case. As a consequence, the reflected wave's spectrum is divided by the incident wave within $w^* \in$ (0, 2.7) to obtain the variations of $\tilde{C}_{ref\_M}$, numerically.

Table 3 Sigmoid-shaped impulse oscillations parameters for Case 2

Case No.	c_1	c_2	T_v (s)
2A	15	0.5	2
2B	150	0.05	0.2
2C	1500	0.005	0.02

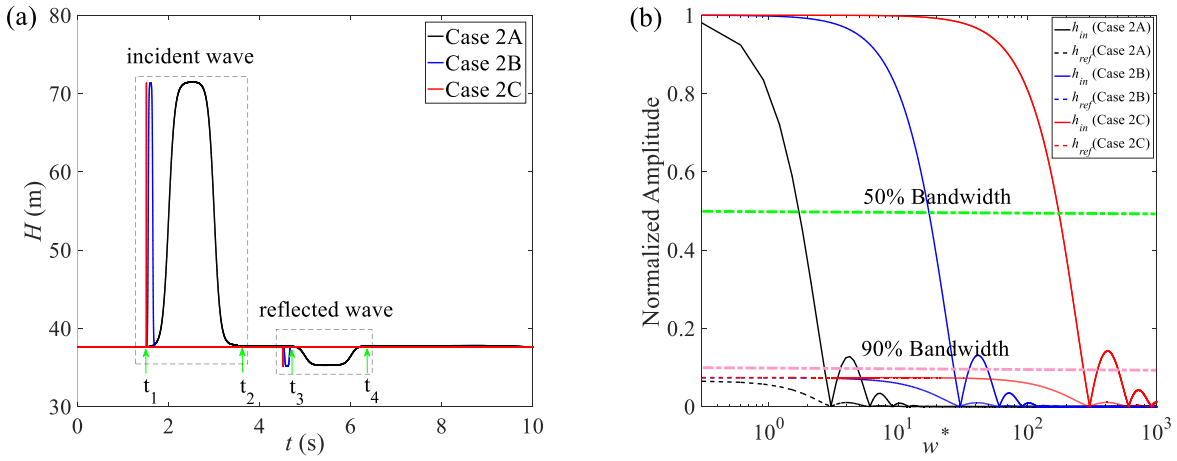

Figure 6 (a) Pressure trace at the measurement location in the time domain; (b) the spectrum of the incident and reflected wave for Case 2

The same system parameters are substituted into the analytical expression of the reflection coefficient to compare the result as seen in Figure 7(a). The green and pink vertical dash-dot lines in this figure indicate the 50% and 90% effective bandwidth for each excitation (notice that the effective bandwidth of impulse signals can also be roughly approximated by $1/Tv$ in the application [47, 53] which is consistent with this bandwidth representaiton). As seen, for the impulses with shorter T_v, such as Case 2B and Case 2C, minor error (less than 3%) occurs in the 50% bandwidth while relatively more significant error (approximately 10%) occurs in the 90% bandwidth. This phenomenon associates with the frequency dependency of the reflection coefficient (i.e., wave number term in Eq. (7) and Eq. (19)), which in the analytical formulae is altered due to the

linearization (Eq. (A.1)). This dependency on the frequency is properly captured by the MOC because it computationally takes the nonlinear effect into account. However, this effect is eliminated as the nonlinear steady friction term is linearized during the derivation of the analytical formula. Figure 7(b) indicates that the maximum error between analytical and numerical results is less than 10% for the 90% bandwidth.

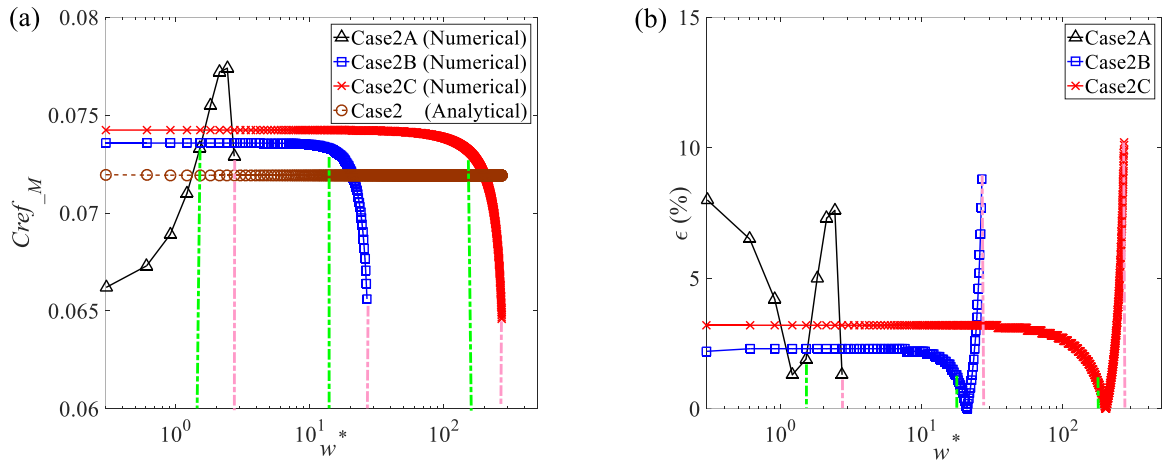

Figure 7 Numerical results for Case 2: (a) leak-induced reflection coefficient; (b) the relative error

3.2 Comparison with a laboratory experiment

The laboratory experiment in [54] is used to validate the proposed analytical solution for the leak-induced reflection coefficient at one measurement point. In this test system, the pipe material is copper, with length L = 37.45 m, inner diameter D = 22.1 mm, and wave speed a = 1328 m/s, which is rounded by the preliminary measurement results from two transducers [55]. It is bounded by a constant level reservoir at upstream and a fully closed in-line valve at downstream, as depicted in Figure 8. The leak is simulated by an orifice with a lumped discharge coefficient $C_d A_L = 1.6\times10^{-6}$ m^2, which locates at y_L = 9.39 m from the in-line valve. Transient is generated by the pulse oscillation

close-open-close of a solenoid valve placed at y_M = 0.05 m from the in-line valve. Detailed test configurations are summarized in Table 4.

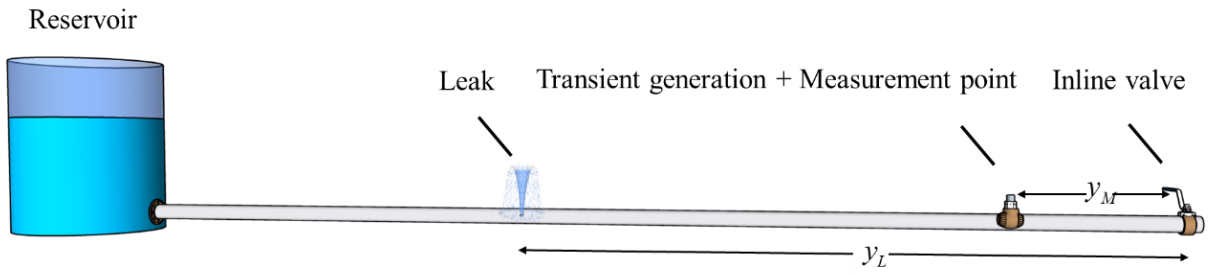

Figure 8 Experimental RPV system with a single leak adopted in [54]

Table 4 Experimental test system settings ([54])

L (m)	D (mm)	a (m/s)	y_L (m)	F_{th} (Hz)	C_dA_L (m^2)	y_M (m)	Input Signal Type	T_v (ms)
37.45	22.1	1328	9.39	8.87	1.6×10^{-6}	0.05	impulse	5.5

In this experiment, it is worthy of noting that (i) the transient measurement point and the transient generation point are identical; (ii) the transient generation point is so adjacent to the closed in-line valve so that its response is influenced by the reflection from the in-line valve (dead-end whose reflection coefficient is 1.0);. (iii) in the leaking test (H_{leak}), additional non-leak reflection/vibration, stemming from pipe bends, internal partial blockage or roughness and pipe material properties, captured by the sensor is epistemic uncertainty [54]. Epistemic uncertainty is changing when experiments are conducted at different time, seasons, or exhaust conditions. So as to minimize its influence on the measured signal, another intact test data (H_{intact}) is used as preference value, i.e., the head difference $\Delta H = H_{intact} - H_{leak}$ is applied to analyze the reflection information.

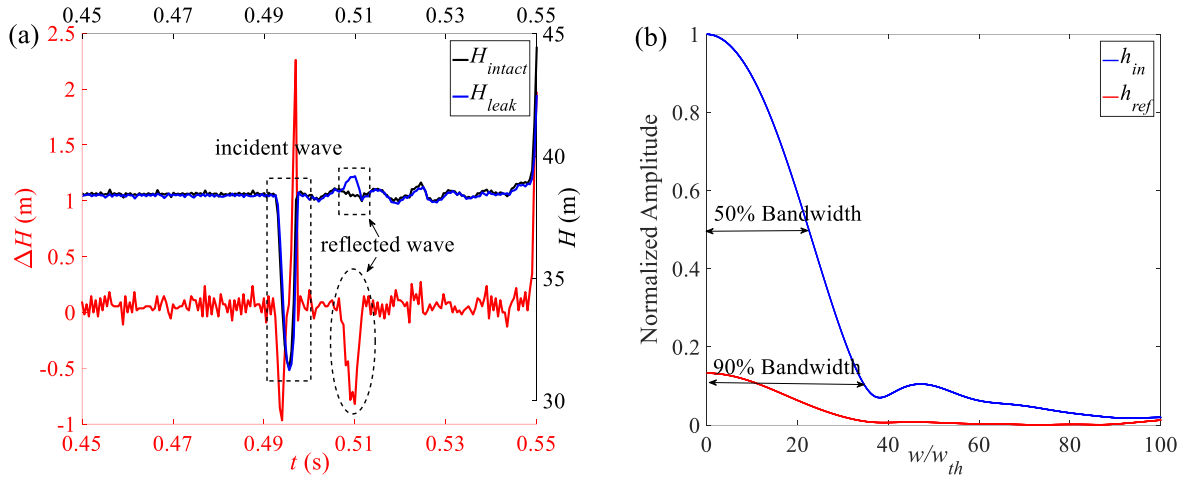

Figure 9 Experimental test results: (a) pressure trace at the measurement location in the time domain; (b) spectrum of the incident and reflected wave

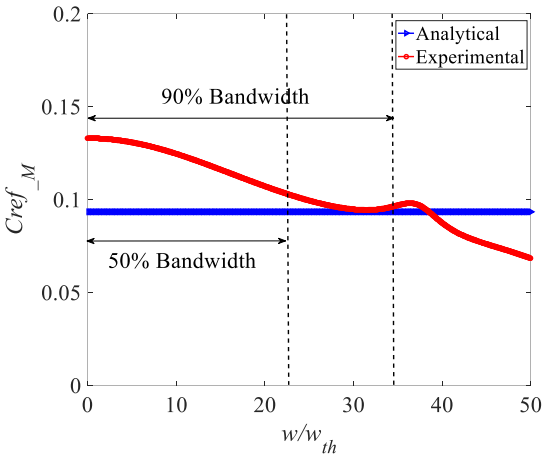

Figure 10 Comparison of the analytical and experimental leak-induced reflection coefficient.

Theoretically, ΔH for the incident wave duration should be zero for a same transient operation (solenoid valve opening and duration), however, due to the epistemic uncertainty in practical cases, we observed non-zero value of ΔH. Reflection coefficient is calculated as following: leak-induced reflection signal is extracted from ΔH (marked by ellipse in Figure 9(a)) while keeping the incident wave in the leaking case (marked by rectangle in Figure 9(a)). Results are plotted in Figure 10. Based on the explained signal extraction procedure, the actual incident wave and reflected wave

in Figure 9(a) are transformed into the frequency domain by FFT as seen in Figure 9(b) to obtain $\tilde{C}_{ref\_M}$ and then compare it with the analytical results (see Figure 10). It shows that in about 90% bandwidth (w = 0~35 w_{th}), the experimental result are closer to the proposed analytical formula as the frequency increases. However, large discrepancies occur in the higher frequency bandwidth (such as 90% of bandwidth).

3.3 Computational impact analysis of the reflection coefficient

Based on the derived reflection coefficient C_{ref_M} in Eq. (16), the association of the leak size and the measurement point is clear. However, in several TRM-based applications, e.g. [17, 29, 45, 47], the friction-induced damping of the wave is neglected or weak. It literally means that they consider the measured reflection coefficient at the leak equal to that at the measurement point. This assumption puts a significant drawback on the developed methods, especially as the leak location is the primary concern in a leak detection exercise. Termed as the line packing effect [48, 56], the friction-induced pressure rise (in the time domain) is even of significant concern for proper water hammer simulation of long-distance oil pipelines [57, 58]. To this end, the parameters affecting the derived damping coefficient are investigated in this section.

3.3.1 Influence of signal measurement distance

Let η denote the friction-induced simplification error, which increases with the distance between the leak and measurement station:

$$\eta(\%) = \left| \frac{C_{ref\_M} - C_{ref\_L}}{C_{ref\_M}} \right| \times 100 \tag{22}$$

In order for its quantification, a long numerical pipeline (L = 10,000 m, D = 0.2 m, Q_{S0} = 0.015 m^3/s, H_{U0} = 40 m, f_D = 0.015) with leakage (y_L^* = 0.9, α = 0.15) for varied measurement location

range (y_M^* = 0.1~0.9) is considered to better understand the importance of this modification.

Figure 11(a) plots the numerical and analytical reflection coefficient variation with the measurement distance for a fixed leak size and location. The relatively small error (within 3%) between the two methods demonstrates the accuracy of the derived analytical formula. It can be seen that the reflection coefficient approximately decreases linearly with the measurement distance. As shown in Figure 11(b), when the distance $d = (y_L^*-y_M^*)L$ is less than 1km, the error is less than 5% which implies neglecting the damping is acceptable. However, as the distance increases up to 10 km, the simplification error rises to 30%, demonstrating its contribution to the defect detection problem.

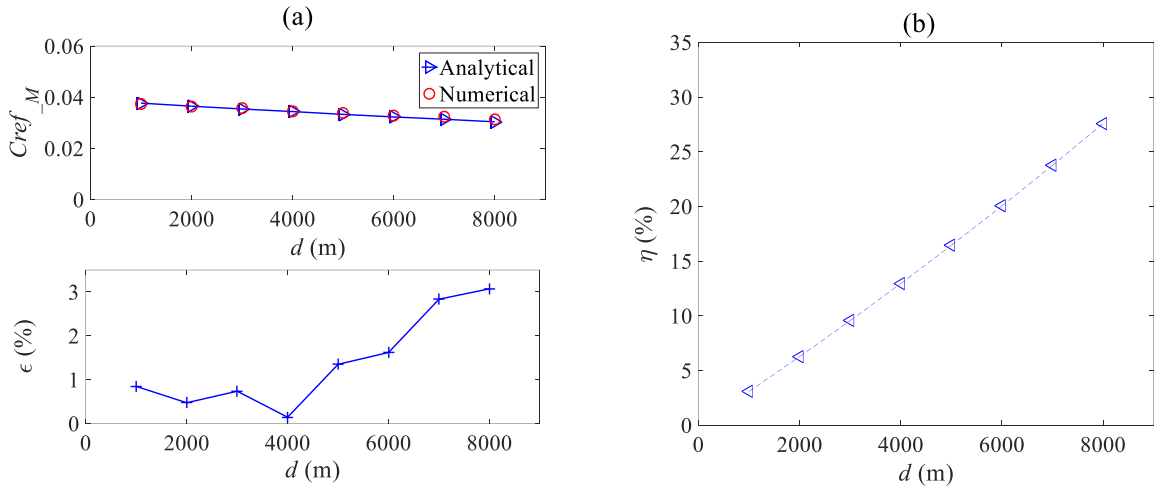

Figure 11 Influence of measurement distance on the reflection coefficient

3.3.2 Influence of initial flow conditions

The derived analytical formula indicates that the initial flow condition (i.e., f_DRe) not only affects the reflected wave f_1 at the leak, which further changes C_{ref_L} but also impacts the damping term μ_j for a given leaky pipe system (constant leakage factor), thus altering C_{ref_M}. To quantify the trend of this impact, the piping system listed in Case 1 in Table 1 is considered for illustration. In

order to obtain more evident reflection signals, the leak factor α is changed from 0.15 to 0.3, which corresponds to the upstream flow rate Q_{S0} variation in the range $5.0\times10^{-4} \sim 4.0\times10^{-2}$ m^3/s (i.e., $\mathrm{Re} \cong 2700 \sim 190000$) while the other parameters are kept unchanged. Figure 12(a) shows a slight rise of C_{ref_M} with $f_D\mathrm{Re}$ along with the corresponding error between the analytical and numerical results.

The comparison indicates the maximum error between the numerical and analytical reflection coefficient is less than 1.5%, in the tested initial flow range. This result firstly confirms the validity of the proposed analytical formula. Furthermore, as seen in Figure 12(b), small $f_D\mathrm{Re}$ (e.g., less than 1,000) has a tiny influence on the difference between C_{ref_L} and C_{ref_M} (i.e., $\eta < 5\%$) but for larger $f_D\mathrm{Re}$ (e.g., greater than 3,000), the difference is more significant than 10% which implies the necessity of modifying the frictionless reflection coefficient $C^{FL}_{ref\_M}$.

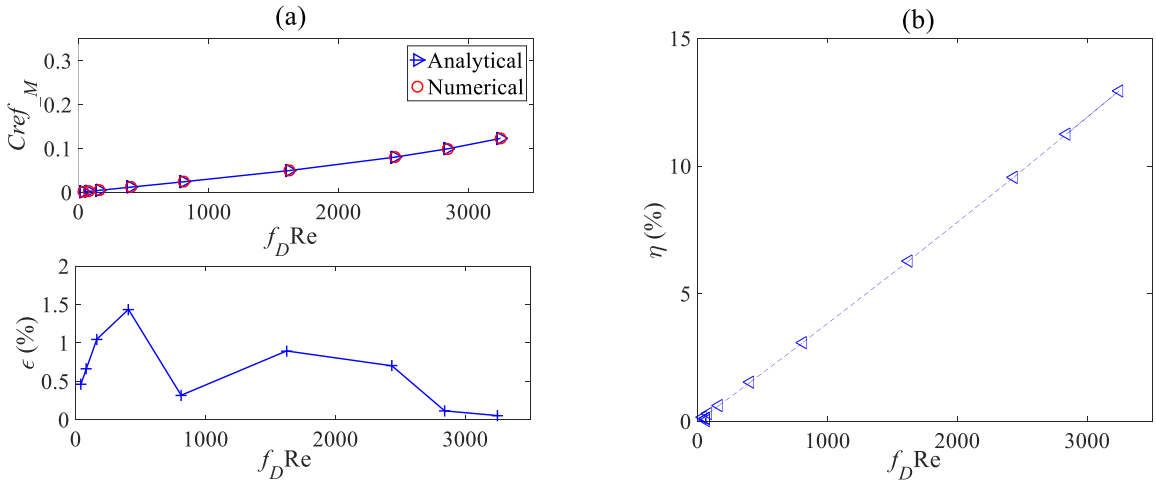

Figure 12 Influence of initial condition on the reflection coefficient

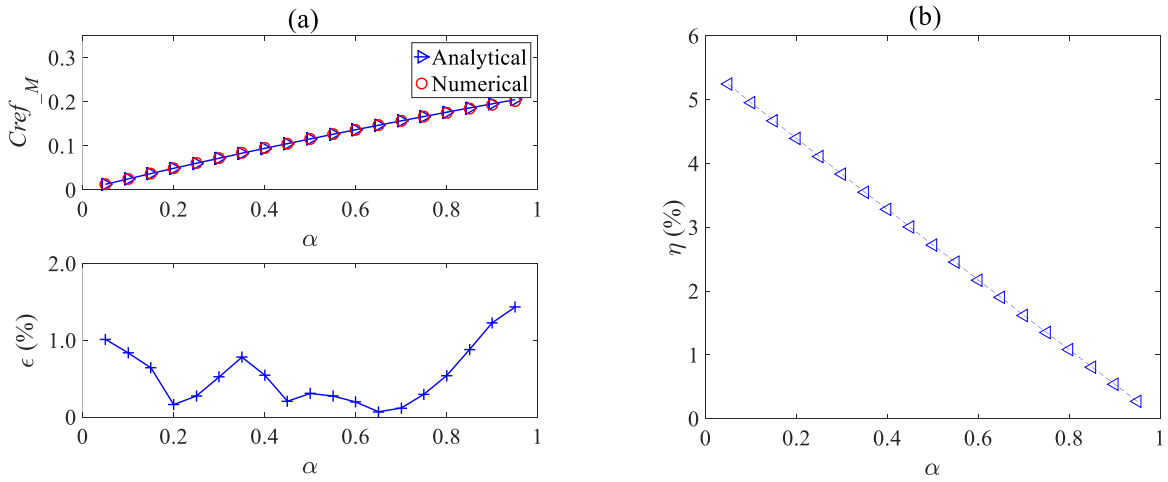

Figure 13 Influence of leak size on the reflection coefficient

3.3.3 Influence of leak size

Leak size is characterized herein by the ratio of discharge from the orifice to its upstream flow rate, i.e., $\alpha = Q_{L0}/Q_{S0}$. Obviously, larger α means a more evident reflection signal for a fixed measurement point. Roughly speaking, a linear relationship between C_{ref_M} and α is seen in Figure 13(a), considering the parameters listed in Table 1 for Case 1, and that trend is confirmed by the MOC results. As expected, in Figure 13(b), the trend of η with α is decreasing because the flow velocity between the leak and measurement point slows down as more flow is leaked (i.e., α increases), which causes reduced frictional damping. Nevertheless, the amount of damping, i.e., the difference for C_{ref_L} and C_{ref_M}, is small (less than 5%) for this system.

4. Dominance Analysis Results and Discussion

Analytical expression tests show that the following quantities impact the reflection coefficient at the measurement point: fluid properties, pipe parameters, initial/steady-state conditions, leak location and size, and transient operation, therefore:

$$C_{ref\_M} = C_{ref\_M}\left(\overbrace{\rho, \upsilon}^{\text{fluid properties}}; \overbrace{L, D, f_D, a}^{\text{pipe parameters}}; \overbrace{Q_{S0}, H_{U0}}^{\text{initial conditions}}; \overbrace{x_L, Q_{L0}}^{\text{leak}}; \overbrace{\Delta H, w_{in}}^{\text{transient source}}\right) \tag{23}$$

In addition, the above-mentioned analysis (Figures 5, 7, 11~13) indicates that the discrepancy between the analytical and the numerical (MOC) reflection coefficient in the 50% dimensionless frequency bandwidth is slight. Furthermore, the significance of the unsteady friction in this testing and analysis range is negligible [59] (also as shown is Figure C.2 in Appendix C). This range of frequencies is also consistent with the actual practice of the TRM using plane waves because high frequencies (sharp waves) excite radial modes which are governed by 2D/3D transient models. Because these high frequencies waves are quickly damped, they are currently less used for defect detections. On this point, the following dominance analysis is based on the low bandwidth frequencies (less than $w^* \approx 10$), which can more accurately simulate the practical case.

Considering Eq. (23) and given empirical perceptions, four dimensionless quantities are introduced to handle the importance of influential factors properly,

$$\alpha = \frac{Q_{L0}}{|Q_{S0}|} \ , \ \ s = \left| \frac{x_M - x_L}{x_M} \right| = \left| \frac{d}{x_M} \right| , \ \ I = f_D \frac{L}{D} \frac{V_0}{a} , \ \ \beta = \frac{\Delta H}{H_{U0}} \tag{24}$$

Consequently, Eq. (23) is rewritten in the following dimensionless form:

$$C_{ref\_M} = C_{ref\_M}(\alpha, s, I, \beta) \tag{25}$$

To arrive at a global measure of importance for the defined four non-dimensional predictors, an explicit expression for the criterion (the leak reflection) in terms of the four parameters is necessary [47-49]. To this end, a nonlinear multiple regression model is developed to fit the analytical formula in Eq. (16). In other words, Eq. (16) now has the role of collected data by which the dominance analysis based on multiple regression is applied.

Considering the common turbulent flow condition in the field conditions, V_0 is set to 0.5~2.5 m/s for circular pipe flow, a is 1000 m/s for the rigid pipe, f_D = 0.015, several system scales (L/D = 500~25,000) are chosen to simulate the leak-induced reflection under different leakage scenario and measurement locations. The independent sets of variables set are summarized in Table 5.

Considering the range of the values used in the sampling, the estimated P value is considerable, meaning that the unsteady friction impact is not significant for all these test cases (compared to steady friction component). Accordingly, this importance assessment primarily targets the transmission mains so that the turbulence structure of the flow during transients is negligible.

Table 5 Detailed parameters for the reflection coefficient C_{ref_M} calculations

Variables	Definition	Range	Sample interval
α	leakage factor	0.05~0.95	0.05
s	leak distance from measurement	0.05~1.00	0.05
I	lumped system parameter	0.00375~0.9375	0.0015
β	transient intensity	0.01~2.42	0.01

Based on the defined dimensionless parameters, in combination with the preliminary observations on the variations of $C_{ref\_M} \sim d$, $C_{ref\_M} \sim f_D\mathrm{Re}$ and $C_{ref\_M} \sim \alpha$ formerly in this study, the following expression is suggested to fit the analytical formula:

$$\left(C_{ref\_M}\right)_{fitted} = \lambda_0 + \lambda_1\alpha^{c_1} + \lambda_2 s^{c_2} + \lambda_3 I^{c_3} + \lambda_4\beta^{c_4} \tag{26}$$

To this aim, the user-defined function called *lsqcurvefit* in Matlab R2016a is implemented in its least-squares mode to achieve the *resnorm* minimization [60]. The fitting degree of the model is evaluated by the statistic Pseudo-R^2 [61] which is related to the sum of squares as follows [62]:

$$\mathrm{Pseudo}-R^2 = 1-\frac{SS_{\mathrm{residual}}}{SS_{\mathrm{total}}} \tag{27}$$

where:

$$SS_{\mathrm{residual}} = \sum_{i=1}^{N}\left(C_{ref\_M,i} - \left(C_{ref\_M}\right)_{\mathrm{fitted},i}\right)^2;$$

$$SS_{\mathrm{total}} = \sum_{i=1}^{N}\left(C_{ref\_M,i} - \bar{C}_{ref\_M}\right)^2;$$

$$\bar{C}_{ref\_M} = \frac{\sum_{i=1}^{N} C_{ref\_M,i}}{N} \tag{28}$$

The closer Pseudo-R^2 to 1.0, the less SS_{residual}, which means a better-fitted model.

Nearly 280,000 cases are run for the data generation in order to simulate various field situations. The regression parameters in Eq. (25) and corresponding Pseudo-R^2 value are λ_0 = −38.9278, λ_1 = 0.3622,c_1 = 1.6315, λ_2 = −0.0295, c_2 = 0.8298, λ_3 = 0.0467, c_3 = 2.6914, λ_4 = 38.9755, c_4 = 0.0016, and Pseudo-R^2 = 0.9395, respectively. The obtained pseudo determination coefficient is quite close to unity, meaning that the fitted function is a good representative of the data (the leak reflection formula). Furthermore, this fitting result indicates that $(C_{ref\_M})_{fitted}$ is positively correlated with α and I while negatively correlated with s which is consistent with the findings on the relation between C_{ref_M} and α, and that between f_DRe and d as observed in Figures 11-13.

To provide a pragmatic inference on the implemented multiple regression analysis, the variations of C_{ref_M} with different factors are plotted in Figure 14. In Figure 14(a), for a given value of the leakage factor α = 0.3, the influence of dimensionless distance s, lumped dimensionless system parameter I, which describes the system scale and initial conditions and transient intensity β on the reflection coefficient C_{ref_M} has been visualized by colors. The warmer the color of the solid circle, the greater the value of C_{ref_M}. The higher value of I, β and smaller s indicates higher C_{ref_M}. This variation trend is also in good agreement with what the nonlinear model predicts. Similarly, Figures 14(b)~(d) demonstrate the variations of C_{ref_M} against the three factors while the remaining parameters are fixed.

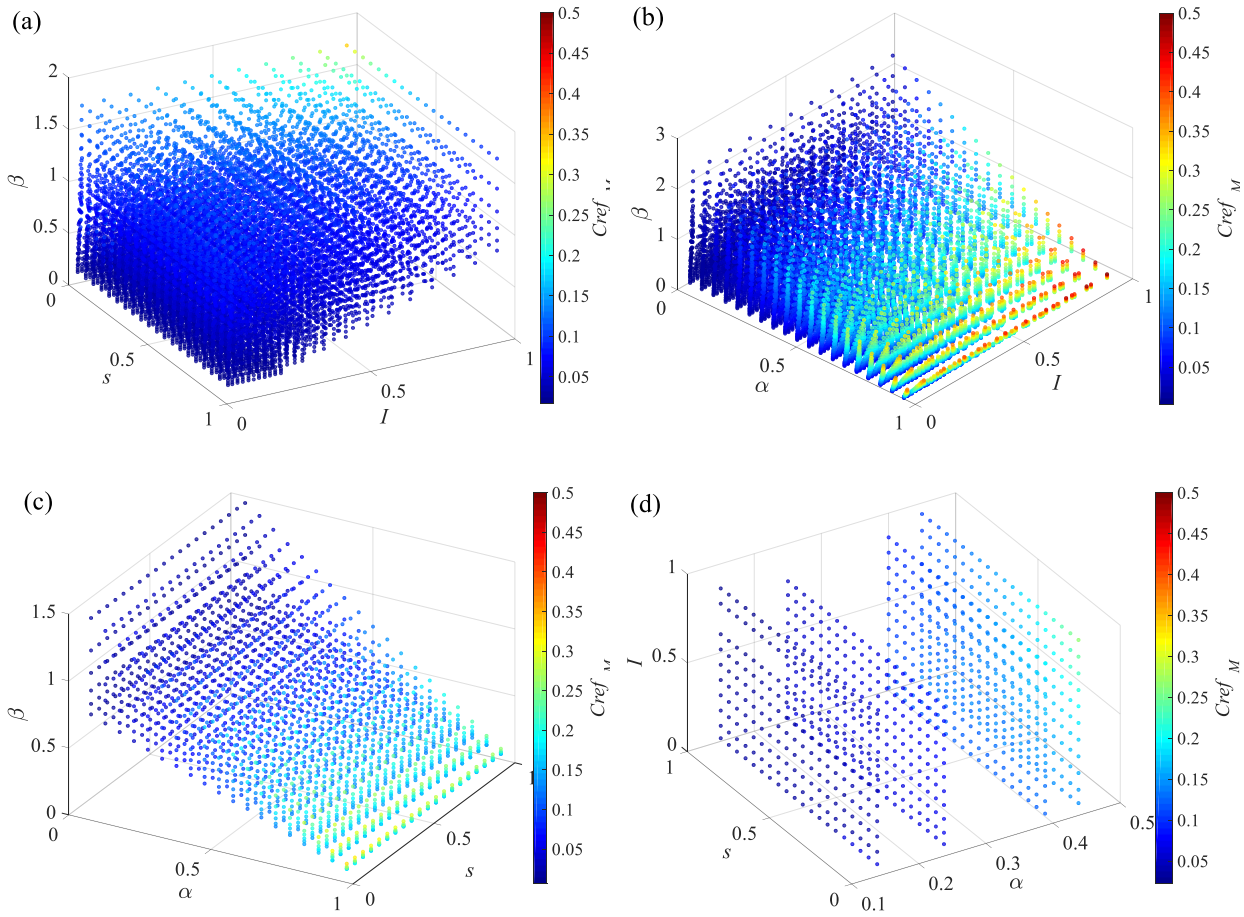

Figure 14 Variations of the reflection coefficient C_{ref_M} (notice the colorbars for the definition of the colors), for the fixed values of one predictor i.e., (a) α = 0.3, (b) s = 0.5, (c) I = 0.5, (d) β = 1.0, and different values of the other predictors.

Based on this full nonlinear regression model, dominance analysis has been conducted to evaluate the relative importance of independent variables/predictors. More results of the implemented procedures are provided in Table 6. As detailed, the first step seeks to fit the raw dataset (nearly 280,000 C_{ref_M}) to all the subset models as shown in the first column in Table 6. It illustrates the significance of the four independent variables (i.e., α, s, I, β) along with the corresponding Pseudo-R^2 as listed in the second column. The remaining columns outline the additional increment of Pseudo-R^2 when the other independent variable is added to this subset

model. Finally, the overall average contribution of each predictor is obtained by averaging different size subset model values. A more substantial overall average value means more importance of the predictor on the full model. For instance, the penultimate row indicates that the contribution of the leakage factor α is 0.3209, which can also be interpreted as the marginal contribution of the variable to the Pseudo-R^2 is 0.3209 while the contribution of the dimensionless distance s is 0.1597. Consequently, according to the last row, the ranking of the four predictors, or their relative importance, is $\alpha > \beta > I > s$.

It is clear that the larger the reflection coefficient, the enhanced leakage detectability. Accordingly, the extensive simulated leaky scenarios using the DA approach provide useful knowledge on detectability in real practice. As a primitive inference from the perspective of the water supply authorities and detection operation companies, decreasing the system pressure, i.e., smaller H_{U0} for the same amplitude of the incident wave, improves the detection exercise, which is consistent with the finding of [63]. Likewise, enhancing the amplitude of transient perturbations, i.e., more prominent ΔH in the appropriate range [64] for fixed system pressure, contributes to the observation and identification of leak reflectivity by increasing transient intensity (as seen in Eq.(26)). However, a trade-off is required to consider in practical applications: the injected signal should impose profound changes to the original flow conditions [65], but on the other hand, large transients severely contaminate the collected data by ambient noise or other random fluctuations.

The reported global importance measures for the TRMs are also of practical significance in managing various leak detection methods and helps toward proper decision making among available choices [71-72]. For example, given the properties and specifications of the field under consideration, the knowledge on the certainty level of each of the four dimensionless parameters can help characterize the confidence level of the results if TRMs are incorporated [73]. Then,

having done a similar DA for other leak detection methods allows rendering more solid decisions among various alternatives.

Table 6 Dominance analysis for the reflection coefficient with four predictors

Model Component	**Pseudo-R^2**	**Added contribution of different factors**			
		α	s	I	β
Null and k = 0 average	0.0000	0.8311	0.6391	0.6693	0.6611
α	0.8311	/	0.0029	0.0331	0.1111
s	0.6391	0.1949	/	0.0331	0.0248
I	0.6693	0.1949	0.0029	/	0.0479
β	0.6611	0.2811	0.0028	0.0561	/
N = 1 average		0.2236	0.0029	0.0408	0.0613
α, s	0.8340	/	/	0.0331	0.1095
α, I	0.8642	/	0.0029	/	0.0806
α, β	0.9422	/	0.0013	0.0026	/
s, I	0.6722	0.1949	/	/	0.0478
s, β	0.6639	0.2796	/	0.0561	/
I, β	0.7172	0.2276	0.0028	/	/
N = 2 average		0.2340	0.0023	0.0306	0.0793
α, s, I	0.8671	/	/	/	0.0724
α, s, β	0.9435	/	/	-0.0040	/
α, I, β	0.9448	/	-0.0053	/	/
s, I, β	0.7200	0.2195	/	/	/
N = 3 average		0.2195	-0.0053	-0.0040	0.0724
α, s, I, β	0.9395	/	/	/	/
Overall average		0.3771	0.1597	0.1842	0.2185
Percentage of Contribution (%)		**40.13**	**17.00**	**19.60**	**23.26**

It is also noted that a comparison of the regressions for $N = 3$ and $N = 4$ in Table 6 reveals that employing three parameters ($N = 3$) provides a better fit than $N = 4$ in some cases. More specifically, incorporating α, s, β or α, I, β leads to Pseudo-$R^2 = 0.9435, 0.9448$ respectively, while regressions using all these four parameters, α, s, I, β, gives Pseudo-$R^2 = 0.9395$. It intuitively means the additional parameter (*s or I* for $N = 3$) does not improve the regression. The reason is that the newly added parameter is not independent, but its contribution may be covered partially by the other (already existing) parameters. Under this condition and considering the defined fitting function in Eq. (26), it is expected to obtain $\lambda_2 \approx 0$ or $\lambda_3 \approx 0$ for $N = 4$, which is actually consistent with the reported values in Table 6. That is, $\lambda_2 = -0.0295$, $\lambda_3 = 0.0467$, which are much smaller than others, $\lambda_0 = -38.9278$, $\lambda_1 = 0.3622$, $\lambda_4 = 38.9755$. It is also worthy of noting that the applied nonlinear regression solves a non-convex optimization problem that may easily be trapped in local minima, especially around the actual (global) optimum. However, such complex optimization problem is out of the scope of current study.

5. Summary and Conclusions

This study establishes the analytical solution for the leak-induced reflection wave at the measurement point in an unbounded water-filled rigid pipeline. The quasi-steady friction, an orifice leakage, and the steady-state flow characteristics are considered for solving wave equations and finding the imposed leakage-induced damping. Several numerical investigations are conducted to verify the derived analytical formula against the MOC solution. Besides, the data of laboratory experiments from the literature are scrutinized to validate the analytical equation.

The derived closed-form formula is then fitted to an exponential function made of the essential dimensionless quantities using the nonlinear multiple regression approach, with an

adequate R^2 quantity being fairly close to unity. A systematic importance analysis based on nearly 280,000 leaky scenarios is conducted to explain the relative importance of different factors on the leak-induced reflection wave. The results demonstrate this importance ranking: leakage factor > transient intensity > lumped system parameter > measurement distance from the leak.

The reported importance order allows for a deeper insight into the performance of the transient-based methods of leak detection if the uncertainty level of the essential dimensionless coefficients in a specific leak detection exercise is known. Moreover, the estimated importance values for the TRMs in comparison with similar values of other methods enable systematic decision-making and leakage detection management.

Further laboratory experiments are required to validate the derived reflection coefficient, and hence the applicability of the fitted exponential function and findings of the performed dominance analysis. A similar investigation for the viscoelastic pipes will be of great value as the damping effect of these pipes is significant and extensively impacts the reflected waves. Therein, the influence of creep coefficients on the leak-induced reflection wave and the consequence on damping seems to lead to improved leak detections in viscoelastic pipes.

Acknowledgments

This research work was supported by the Hong Kong Research Grant Council (projects No. 15200719 and No. 15201017).

Appendix – Analytical Derivations

(A) Transient wave equation with quasi-steady friction

In engineering fields, turbulent flow occurs more frequently than the laminar one [66], so in the following part, derivations are giving in detail based on turbulent flow. If the flow perturbation q^*

is much smaller than Q_0, there is

$$Q^2 = \left(Q_0 + q^*\right)^2 \approx Q_0^2 + 2Q_0 q^* \tag{A.1}$$

in which nonlinear term $\left(q^*\right)^2$ which does not influence location of a leak but affects friction damping [26] is ignored. Under the assumption of relatively small-amplitude perturbation and linearization, Eqs. (1) and (2) are finally transformed into

$$\frac{\partial h^*}{\partial t} = -\frac{a^2}{gA}\frac{\partial q^*}{\partial x} \tag{A.2}$$

$$\frac{\partial h^*}{\partial x} = -\frac{1}{gA}\frac{\partial q^*}{\partial t} - R \cdot q^* \tag{A.3}$$

where $R = f_D Q_0 \big/ \left(gDA^2\right)$ for turbulent flow. $\partial(Eq.(\text{A.2}))/\partial x - \partial(Eq.(\text{A.3}))/\partial t$ yields that

$$\frac{\partial^2 q^*}{\partial x^2} - \frac{1}{a^2}\frac{\partial^2 q^*}{\partial t^2} - \frac{gAR}{a^2}\cdot\frac{\partial q^*}{\partial t} = 0 \tag{A.4}$$

Assuming that q^* and h^* are sinusoidal oscillation and can be represented in the exponential form by using the separation of variables methods [28, 67, 68] for its convenience in solving partial derivative equations (PDEs).

$$q^*(x,t) = q\left(x\right)\mathrm{e}^{jwt} \tag{A.5}$$

$$h^*(x,t) = h\left(x\right)\mathrm{e}^{jwt} \tag{A.6}$$

in which $q(x)$ and $h(x)$ are all complex variables and are functions of x only for a given frequency wave, w is the angular frequency in rad/s, j is the imaginary unit.

Substituting Eq. (A.5) and (A.6) into Eq. (A.4), PDE is transformed into an ordinary derivative equation (ODE) (As seen in Eq. (A.7)).

$$\frac{d^2 q}{dx^2} = -\left(\frac{w^2}{a^2} - \frac{jgAwR}{a^2}\right)q \tag{A.7}$$

Or $$\frac{d^2q}{dx^2}+\mu^2 q=0 \tag{A.8}$$

in which $\mu^2=\frac{w^2}{a^2}\left(1-\frac{jgAR}{w}\right)$, with $\mu=\frac{w}{a}\sqrt{1-\frac{jgAR}{w}}=\mu_r+j\mu_j$ being propagation operator, and

$$\mu_r=-\frac{gAwR}{2a^2\mu_j},\ \mu_j=-\frac{w}{a}\sqrt{\frac{-1+\sqrt{1+\left(gAR/w\right)^2}}{2}} \tag{A.9}$$

The real part μ_r and imaginary part μ_j represent phase change and friction-related damping of the traveling wave, respectively [48, 69], which can also be seen in the following section for the derivation of pressure head perturbation. The solution of Eq. (A.8) is

$$q(x)=q^{ref}\mathrm{e}^{j\mu x}+q^{tr}\mathrm{e}^{-j\mu x} \tag{A.10}$$

where q^{tr} and q^{ref} = flow rate corresponding to transmitted wave h^{tr} and reflected wave h^{ref}, respectively. Substituting Eqs. (A.5), (A.6), and (A.10) into Eq. (A.2), there is

$$h(x)=\frac{\mu a^2}{gAw}\left[-q^{ref}\mathrm{e}^{j\mu x}+q^{tr}\mathrm{e}^{-j\mu x}\right]=-h^{ref}\mathrm{e}^{j\mu x}+h^{tr}\mathrm{e}^{-j\mu x} \tag{A.11}$$

where

$$h^{ref}=\frac{\mu a^2}{gAw}q^{ref}=k'q^{ref},\ \ h^{tr}=\frac{\mu a^2}{gAw}q^{tr}=k'q^{tr},\ \ k'=\frac{\mu a^2}{gAw}=jZ_c,\ \ Z_c=\frac{\mu a^2}{jgAw} \tag{A.12}$$

It should be noted that these four variables are complex number. Substituting Eq. (A.11) into Eq. (A.6) yields that

$$h^*(x,t)=h(x)\mathrm{e}^{jwt}=\left(-h^{ref}\mathrm{e}^{j\mu x}+h^{tr}\mathrm{e}^{-j\mu x}\right)\mathrm{e}^{jwt}=f+F \tag{A.13}$$

where $f=-h^{ref}\mathrm{e}^{j(\mu x+wt)}$ = reflected wave, $F=h^{tr}\mathrm{e}^{j(-\mu x+wt)}$ = incident wave.

Similarly, Substituting Eq. (A.10) into Eq. (A.5) yields that,

$$q^*(x,t)=q(x)\mathrm{e}^{jwt}=\left(q^{ref}\mathrm{e}^{j\mu x}+q^{tr}\mathrm{e}^{-j\mu x}\right)\mathrm{e}^{jwt}=\frac{1}{k'}(-f+F) \tag{A.14}$$

Eqs. (A.13) and (A.14) indicate that the perturbation of pressure head and flow rate at arbitrary

space and time point (x, t) can be evaluated by these two traveling wave functions. The combination of Eqs. (A.13) and (A.14) are used to solve the magnitude of the transmitted and reflected wave when a transient pressure wave arrives at a leak.

(B) Leak-induced reflection coefficient without frictional effects

Particularly, if $f_D = 0$, according to Eqs. (A.8) and (A.12), there are

$$\mu = \frac{w}{a},\ k' = \frac{a}{gA} \tag{B.1}$$

Substituting Eq. (B.1) into Eq. (7),

$$f_1 = \frac{1}{8}\frac{\left(\frac{a}{gA}\right)^2 \alpha^2 Q^2_{S0}}{H_{L0}} + \frac{\frac{a}{gA}}{2}\alpha|Q_{S0}| - \frac{1}{2}\frac{\frac{a}{gA}}{2}\frac{\alpha|Q_{S0}|}{\sqrt{H_{L0}}}\sqrt{\left(\frac{\frac{a}{gA}}{2}\frac{\alpha Q_{S0}}{\sqrt{H_{L0}}}\right)^2 + 4\left(\frac{\frac{a}{gA}}{2}\alpha|Q_{S0}| + H_{L0} + F_1\right)} \tag{B.2}$$

For the case of sudden closure of the downstream valve-induced transient wave, the incident wave F_1 becomes

$$F_1 = \frac{a(|Q_{s0}| - Q_{l0})}{Ag} = \frac{a|Q_{s0}|(1-\alpha)}{Ag} \Rightarrow \frac{a|Q_{s0}|}{Ag} = \frac{F_1}{(1-\alpha)} \tag{B.3}$$

Substituting Eqs. (B.2) and (B.3) into Eq. (8) gives,

$$\begin{aligned} C^{FL}_{ref\_L} &= \frac{\frac{1}{8}\frac{\left(\frac{aQ_{S0}}{gA}\right)^2 \alpha^2}{H_{L0}} + \frac{a|Q_{S0}|}{gA}\frac{\alpha}{2} - \frac{1}{4}\frac{\alpha}{\sqrt{H_{L0}}}\frac{a|Q_{S0}|}{gA}\sqrt{\left(\frac{aQ_{S0}}{gA}\frac{\alpha}{2\sqrt{H_{L0}}}\right)^2 + 4\left(\frac{a|Q_{S0}|}{gA}\frac{\alpha}{2} + H_{L0} + F_1\right)}}{F_1} \\ &= \frac{\frac{1}{8}\frac{\frac{F_1^2}{(1-\alpha)^2}\alpha^2}{H_{L0}F_1} + \frac{F_1}{(1-\alpha)}\frac{\alpha}{2F_1} - \frac{1}{4}\frac{\alpha}{\sqrt{H_{L0}}}\frac{F_1}{(1-\alpha)F_1}\sqrt{\left(\frac{F_1}{(1-\alpha)}\frac{\alpha}{2\sqrt{H_{L0}}}\right)^2 + 4\left(\frac{F_1}{(1-\alpha)}\frac{\alpha}{2} + H_{L0} + F_1\right)}}{} \\ &= 2\left(\frac{\alpha}{4(1-\alpha)}\right)^2\frac{F_1}{H_{L0}} + 2\frac{\alpha}{4(1-\alpha)} - \frac{\alpha}{4(1-\alpha)}\sqrt{4\left(\frac{F_1}{(1-\alpha)}\frac{\alpha}{4H_{L0}}\right)^2 + 4\left(\frac{F_1}{(1-\alpha)H_{L0}}\frac{\alpha}{2} + 1 + \frac{F_1}{H_{L0}}\right)} \\ &= 2\delta^2\chi + 2\delta - 2\delta\sqrt{(\chi\delta+1)^2 + \chi)} \end{aligned} \tag{B.4}$$

where

$$\chi = \frac{F_1}{H_{L0}}, \quad \delta = \frac{\alpha}{4(1-\alpha)} \tag{B.5}$$

(C) Transient wave equation with unsteady friction

The one-dimensional governing equations containing unsteady friction effect are expressed in [48, 70]

$$\frac{gA}{a^2}\frac{\partial H}{\partial t} + \frac{\partial Q}{\partial x} = 0 \tag{C.1}$$

$$\frac{\partial Q}{\partial t} + gA\frac{\partial H}{\partial x} + \frac{\pi D}{\rho}\tau_w = 0 \tag{C.2}$$

where ρ = fluid density; τ_w = pipe wall shear stress = τ_{ws} + τ_{wu}, in which τ_{ws} and τ_{wu} represents the steady and unsteady shear stress component for turbulent flow.

Transforming Eq. (C.1) and Eq. (C.2) into the frequency domain (more details please refer to [70])

$$\frac{gA}{a^2}(jwh) + \frac{\partial q}{\partial x} = 0 \tag{C.3}$$

$$\frac{1}{gA}(jwq) + \frac{\partial h}{\partial x} + \left[\frac{f_D Q_0}{gDA^2} + \frac{f_D q_0^*}{2gDA^2}\right]q + jw\frac{16\upsilon}{gAD^2}\frac{\varphi}{\sqrt{\pi(\lambda + jw)}}q = 0 \tag{C.4}$$

$\frac{\partial(\text{Eq.(C.3)})}{\partial x} - \left(\frac{gA}{a^2}jw\right) \times \text{Eq.(C.4)}$, we have

$$\frac{\partial^2 q}{\partial x^2} + \mu_E{}^2 q = 0 \tag{C.5}$$

in which $\mu_E = \frac{w}{a}\sqrt{1 - jR_E}$, $R_E = R_{S1} + R_{S2} + R_U$ with R_{S1}, R_{S2} and R_U being quasi-steady (first-order), nonlinear (second-order) and unsteady friction components of extended friction resistance factor R_E, respectively. Specifically, they have following forms [70]:

$$R_{S1} = \frac{f_D Q_0}{wDA}; R_{S2} = \frac{f_D q_0}{2wDA}; R_U = \frac{16 j\upsilon\varphi}{D^2\sqrt{\lambda + jw}} \tag{C.6}$$

Let $\mu_E = \mu_{E,r} + j\mu_{E,j}$, $R_U = R_{U,r} + jR_{U,j}$ and take square both sides of the expression μ_E, there is

$$\mu_{E,r}^2 - \mu_{E,j}^2 + j2\mu_{E,r}\mu_{E,j} = \frac{w^2}{a^2}\left[1 + R_{U,j} - j\left(R_{S1} + R_{S2} + R_{U,r}\right)\right] \tag{C.7}$$

$$\begin{cases} \mu_{E,r}^2 - \mu_{E,j}^2 = \dfrac{w^2}{a^2}\left(1 + R_{U,j}\right) = AA \\ 2\mu_{E,r}\mu_{E,j} = -\dfrac{w^2}{a^2}\left(R_{S1} + R_{S2} + R_{U,r}\right) = BB \end{cases} \Rightarrow \begin{cases} \mu_{E,r} = \sqrt{\dfrac{AA + \sqrt{AA^2 + BB^2}}{2}} \\ \mu_{E,j} = \sqrt{\dfrac{-AA + \sqrt{AA^2 + BB^2}}{2}} \end{cases} \tag{C.8}$$

in which $R_{U,r} = \dfrac{\sqrt{2}}{2}\dfrac{16\upsilon\varphi}{D^2\sqrt{\lambda^2 + w^2}}\sqrt{\sqrt{\lambda^2 + w^2} - \lambda}$, $R_{U,j} = \dfrac{\sqrt{2}}{2}\dfrac{16\upsilon\varphi}{D^2\sqrt{\lambda^2 + w^2}}\sqrt{\sqrt{\lambda^2 + w^2} + \lambda}$.

In this way, total friction-related damping of the traveling wave is derived (please see $\mu_{E,j}$ in Eq. (C.8)). The numerical results of Case 1 and Case 2C containing all friction terms (notated as SF+UF) are compared with the previous results with only quasi-steady friction term considered (notated as SF), please see Table C1 and Figures C1 and C2 below.

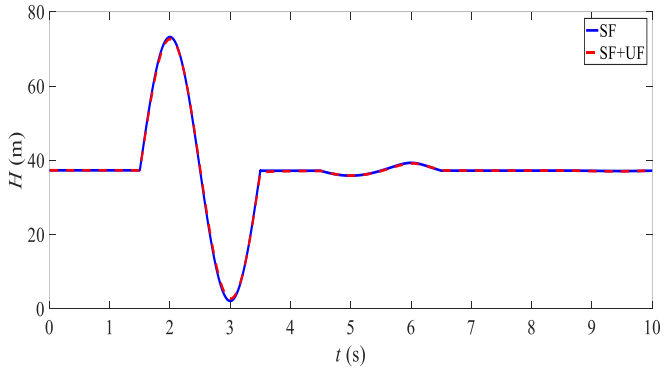

Figure C1 Pressure trace at the measurement location (y_M^*=0.3) for Case 1

Table C1 Numerical results of derived leak-induced reflection coefficient for Case 1

	MOC result (SF)	MOC result (SF+UF)	Relative error (%)
$\left(h_{amp}\right)_M$ (m)	35.91	35.38	1.5

$\left(h_{amp}\right)'_M$ (m)	1.32	1.26	4.6
C_{ref_M} (%)	3.68	3.56	3.2

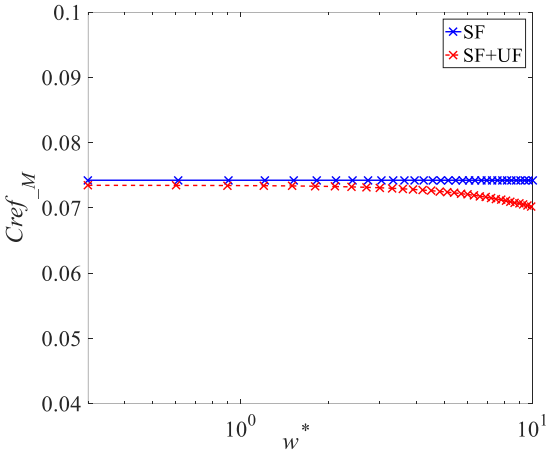

Figure C2 Numerical results for Case 2C

Notations

$\alpha = Q_{L0}/|Q_{S0}|$ = leakage factor;

$\beta = \Delta H/H_{U0}$ = transient intensity;

a = wave speed (m/s);

A = pipe cross-sectional area (m^2);

A_L = orifice area (m^2);

C_d = leak discharge coefficient;

C_{ref_M} = leak-induced reflection coefficient at the measurement point;

D = pipe diameter (m);

d = distance between the leak and the measurement point;

f_D = Darcy-Weisbach friction factor;

f_{in} = frequency of the input transient signal (s^{-1});

f_1 = reflected wave (m);

F_1 = incident wave (m);

F_2 = transmitted wave (m);

$F_{th} = a/(4L)$ = fundamental frequency for a bounded pipe (Hz);

g = gravitational acceleration (m/s);

H_A, H_B = pressure head at point A (leak downstream) and point B (leak upstream) (m);

ΔH_{jou} = Joukowsky head (m);

H_{U0} = steady state pressure head at pipe section upstream end or reservoir/tank (m);

$I = f_D ML/D$ = lumped dimensionless system parameter;

j = imaginary number;

L = pipe length (m);

$M = V_0/a$ = Mach number;

Q_{S0} = initial flow rate at pipe section upstream (m^3/s);

Q_L = leak discharge (m^3/s);

"Real" = real part;

s = dimensionless distance between leak and measurement point;

$T_e = 2d/a$ = wave time scale between the measurement point and the leak point;

w = angular frequency (rad/s);

$w_e = 1/T_e$ frequency corresponding to the length d (rad/s);

$w^* = w/w_e$ dimensionless frequency;

w_{in} = frequency of the input transient signal (rad/s);

$w_{th} = 1/F_{th}$ = fundamental angular frequency for a bounded (rad/s);

x_L = the leak distance from the pipe section upstream (m);

y_L = the leak distance from the pipe section downstream (m);

y_M = the distance between the measurement point and the pipe section downstream (m);

μ_r , μ_j = real and imaginary part of complex-value propagation operator μ ;

0 = subscript for representing steady state.

References

[1] H.F. Duan, B. Pan, M.L. Wang, L. Chen, F.F. Zheng, Y. Zhang, State-of-the-art review on the transient flow modeling and utilization for urban water supply system (UWSS) management, Journal of Water Supply Research and Technology-Aqua, 69 (2020) 858-893.

[2] A. Keramat, M. Payesteh, B. Brunone, S. Meniconi, Interdependence of flow and pipe characteristics in transient induced contamination intrusion: numerical analysis, Journal of Hydroinformatics, 22 (2020) 473-490.

[3] A. Keramat, B. Karney, M.S. Ghidaoui, X. Wang, Transient-based leak detection in the frequency domain considering fluid–structure interaction and viscoelasticity, Mechanical Systems and Signal Processing, 153 (2021) 107500.

[4] M. Fantozzi, N. Bazzurro, M. Mazzola, Progress on implementing the IWA approach in Italy: Case studies, dissemination and training activities of the Italian Water Loss user group and links with European funded projects, Proceedings of IWA Conference'Leakage Management: A Practical Approach', Halifax, Canada, 2005.

[5] T.C. Che, H.F. Duan, P.J. Lee, Transient wave-based methods for anomaly detection in fluid pipes: A review, Mechanical Systems and Signal Processing, 160 (2021) 107874.

[6] A.N. Tafuri, Locating leaks with acoustic technology, Journal-American Water Works Association, 92 (2000) 57-66.

[7] S. Hamilton, B. Charalambous, Leak detection: technology and implementation, IWA Publishing, 2020.

[8] X. Wang, M.S. Ghidaoui, Identification of multiple leaks in pipeline: Linearized model, maximum likelihood, and super-resolution localization, Mechanical Systems and Signal Processing, 107 (2018) 529-548.

[9] X. Wang, M.S. Ghidaoui, Identification of multiple leaks in pipeline II: Iterative beamforming and leak number estimation, Mechanical Systems and Signal Processing, 119 (2019) 346-362.

[10] X. Wang, M.S. Ghidaoui, J.R. Lin, Identification of multiple leaks in pipeline III: Experimental results, Mechanical Systems and Signal Processing, 130 (2019) 395-408.
[11] X. Wang, J.R. Lin, A. Keramat, M.S. Ghidaoui, S. Meniconi, B. Brunone, Matched-field processing for leak localization in a viscoelastic pipe: An experimental study, Mechanical Systems and Signal Processing, 124 (2019) 459-478.
[12] T.C. Che, H.F. Duan, B. Pan, P.J. Lee, M.S. Ghidaoui, Energy analysis of the resonant frequency shift pattern induced by nonuniform blockages in pressurized water pipes, Journal of Hydraulic Engineering, 145 (2019) 04019027.
[13] X. Wang, J.R. Lin, M.S. Ghidaoui, S. Meniconi, B. Brunone, Estimating viscoelasticity of pipes with unknown leaks, Mechanical Systems and Signal Processing, 143 (2020).
[14] H.F. Duan, P.J. Lee, M.S. Ghidaoui, Y.K. Tung, Essential system response information for transient-based leak detection methods, Journal of Hydraulic Research, 48 (2010) 650-657.
[15] S. Meniconi, B. Brunone, M. Ferrante, C. Capponi, Mechanism of interaction of pressure waves at a discrete partial blockage, Journal of Fluids and Structures, 62 (2016) 33-45.
[16] B. Brunone, Transient test-based technique for leak detection in outfall pipes, Journal of Water Resources Planning and Management-Asce, 125 (1999) 302-306.
[17] B. Brunone, M. Ferrante, Detecting leaks in pressurised pipes by means of transients, Journal of Hydraulic Research, 39 (2001) 539-547.
[18] P.J. Lee, J.P. Vítkovský, M.F. Lambert, A.R. Simpson, J. Liggett, Leak location in pipelines using the impulse response function, Journal of Hydraulic Research, 45 (2007) 643-652.
[19] D. Covas, H. Ramos, A.B. De Almeida, Standing wave difference method for leak detection in pipeline systems, Journal of Hydraulic Engineering, 131 (2005) 1106-1116.
[20] H.F. Duan, P.J. Lee, M.S. Ghidaoui, Y.K. Tung, Leak detection in complex series pipelines by using the system frequency response method, Journal of Hydraulic Research, 49 (2011) 213-221.
[21] S.H. Kim, Multiple leak detection algorithm for pipe network, Mechanical Systems and Signal Processing, 139 (2020) 106645.
[22] J. Gong, M.F. Lambert, A.R. Simpson, A.C. Zecchin, Single-event leak detection in pipeline using first three resonant responses, Journal of Hydraulic Engineering, 139 (2013) 645-655.
[23] T.C. Che, H.F. Duan, P.J. Lee, S. Meniconi, B. Pan, B. Brunone, Radial pressure wave behavior in transient laminar pipe flows under different flow perturbations, Journal of Fluids

Engineering-Transactions of the Asme, 140 (2018) 101203.
[24] C. Massari, T.C.J. Yeh, M. Ferrante, B. Brunone, S. Meniconi, A stochastic approach for extended partial blockage detection in viscoelastic pipelines: numerical and laboratory experiments, Journal of Water Supply Research and Technology-Aqua, 64 (2015) 583-595.
[25] S. Meniconi, B. Brunone, M. Ferrante, In-line pipe device checking by short-period analysis of transient tests, Journal of Hydraulic Engineering-Asce, 137 (2011) 713-722.
[26] X.J. Wang, M.F. Lambert, A.R. Simpson, J.A. Liggett, J.P. Vı´tkovský, Leak detection in pipelines using the damping of fluid transients, Journal of Hydraulic Engineering, 128 (2002) 697-711.
[27] B. Brunone, S. Meniconi, C. Capponi, Numerical analysis of the transient pressure damping in a single polymeric pipe with a leak, Urban Water Journal, 15 (2018) 760-768.
[28] E.B. Wylie, Fluid transients in systems, Englewood Cliffs, NJ : Prentice Hall, Englewood Cliffs, NJ, 1993.
[29] L. Jönsson, M. Larson, Leak detection through hydraulic transient analysis, Pipeline systems, Springer, 1992, pp. 273-286.
[30] P.J. Lee, M.F. Lambert, A.R. Simpson, J.P. Vítkovský, J. Liggett, Experimental verification of the frequency response method for pipeline leak detection, Journal of Hydraulic Research, 44 (2006) 693-707.
[31] B. Pan, H.F. Duan, S. Meniconi, B. Brunone, FRF-based transient wave analysis for the viscoelastic parameters identification and leak detection in water-filled plastic pipes, Mechanical Systems and Signal Processing, 146 (2021) 107056.
[32] M. Taghvaei, S.B.M. Beck, W.J. Staszewski, Leak detection in pipelines using cepstrum analysis, Measurement Science and Technology, 17 (2006) 367.
[33] J.D. Shucksmith, J.B. Boxall, W.J. Staszewski, A. Seth, S.B.M. Beck, Onsite leak location in a pipe network by cepstrum analysis of pressure transients, Journal-American Water Works Association, 104 (2012) E457-E465.
[34] S.T.N. Nguyen, J.Z. Gong, M.F. Lambert, A.C. Zecchin, A.R. Simpson, Least squares deconvolution for leak detection with a pseudo random binary sequence excitation, Mechanical Systems and Signal Processing, 99 (2018) 846-858.
[35] M. Ferrante, B. Brunone, S. Meniconi, Wavelets for the analysis of transient pressure signals for leak detection, Journal of Hydraulic Engineering, 133 (2007) 1274-1282.

[36] M. Ferrante, B. Brunone, S. Meniconi, Leak-edge detection, Journal of Hydraulic Research, 47 (2009) 233-241.
[37] C.P. Liou, Pipeline leak detection by impulse response extraction, Journal of Fluids Engineering, 120 (1998) 833-838.
[38] S. Beck, M. Curren, N. Sims, R. Stanway, Pipeline network features and leak detection by cross-correlation analysis of reflected waves, Journal of Hydraulic Engineering, 131 (2005) 715-723.
[39] P.J. Lee, M.F. Lambert, A.R. Simpson, J.P. Vítkovsky, D. Misiunas, Leak location in single pipelines using transient reflections, Australasian Journal of Water Resources, 11 (2007) 53-65.
[40] N.E. Huang, Z. Shen, S.R. Long, M.C. Wu, H.H. Shih, Q. Zheng, N.C. Yen, C.C. Tung, H.H. Liu, The empirical mode decomposition and the Hilbert spectrum for nonlinear and non-stationary time series analysis, Proceedings of the Royal Society of London. Series A: mathematical, physical engineering sciences, 454 (1998) 903-995.
[41] S. Belsito, P. Lombardi, P. Andreussi, S. Banerjee, Leak detection in liquefied gas pipelines by artificial neural networks, AIChE Journal, 44 (1998) 2675-2688.
[42] D.V. Budescu, R. Azen, Beyond global measures of relative importance: Some insights from dominance analysis, Organizational Research Methods, 7 (2004) 341-350.
[43] J.W. Johnson, A heuristic method for estimating the relative weight of predictor variables in multiple regression, Multivariate Behavioral Research, 35 (2000) 1-19.
[44] R. Azen, D.V. Budescu, The dominance analysis approach for comparing predictors in multiple regression, Psychological Methods, 8 (2003) 129-148.
[45] D. Covas, H. Ramos, N. Graham, C. Maksimovic, Application of hydraulic transients for leak detection in water supply systems, Water Science and Technology: Water Supply, 4 (2004) 365-374.
[46] C. Capponi, S. Meniconi, P.J. Lee, B. Brunone, M. Cifrodelli, Time-domain Analysis of Laboratory Experiments on the Transient Pressure Damping in a Leaky Polymeric Pipe, Water Resources Management, 34 (2020) 501-514.
[47] W.J. Wang, Z. Li, L.W. Jing, P. Lee, R. Murch, A straightforward method for estimating the size of leaks in water pipelines using acoustic transients, Journal of the Acoustical Society of America, 144 (2018) EL404-EL409.
[48] M.H. Chaudhry, Applied hydraulic transients, Third edition.. ed., New York : Springer, New

York, 2014.
[49] U. Lorenzo-Seva, P.J. Ferrando, E. Chico, Two SPSS programs for interpreting multiple regression results, Behavior Research Methods, 42 (2010) 29-35.
[50] H.F. Duan, M.S. Ghidaoui, P.J. Lee, Y.K. Tung, Relevance of unsteady friction to pipe size and length in pipe fluid transients, Journal of Hydraulic Engineering, 138 (2012) 154-166.
[51] S. Meniconi, H.F. Duan, B. Brunone, M.S. Ghidaoui, P.J. Lee, M. Ferrante, Further Developments in Rapidly Decelerating Turbulent Pipe Flow Modeling, Journal of Hydraulic Engineering, 140 (2014).
[52] P.J. Lee, H.F. Duan, J. Tuck, M.S. Ghidaoui, Numerical and experimental study on the effect of signal bandwidth on pipe assessment using fluid transients, Journal of Hydraulic Engineering, 141 (2015) 04014074.
[53] J.L. Semmlow, Circuits, signals, and systems for bioengineers a MATLAB-based introduction, Oxford : Academic, Oxford, 2005.
[54] X. Wang, M. Waqar, H.C. Yan, M. Louati, M.S. Ghidaoui, P.J. Lee, S. Meniconi, B. Brunone, B. Karney, Pipeline leak localization using matched-field processing incorporating prior information of modeling error, Mechanical Systems and Signal Processing, 143 (2020) 106849.
[55] P.J. Lee, Using system response functions of liquid pipelines for leak and blockage detection, the University of Adelaide, Adelaide, Australia, 2005.
[56] C.P. Liou, Understanding Line Packing in Frictional Water Hammer, Journal of Fluids Engineering-Transactions of the Asme, 138 (2016) 081303.
[57] C.P. Liou, Pipeline variable uncertainties and their effects on leak detectability, American Petroleum Institute, Washington, DC., 1993.
[58] M. Ludwig, S.P. Johnson, Prediction of surge pressures in long oil transmission lines, Proc. API Div. Transp., 30 (1950) 62-70.
[59] H.F. Duan, M. Ghidaoui, P.J. Lee, Y.K. Tung, Unsteady friction and visco-elasticity in pipe fluid transients, Journal of Hydraulic Research, 48 (2010) 354-362.
[60] J. Lopez-Luna, L.E. Ramirez-Montes, S. Martinez-Vargas, A.I. Martinez, O.F. Mijangos-Ricardez, M.D.A. Gonzalez-Chavez, R. Carrillo-Gonzalez, F.A. Solis-Dominguez, M.D. Cuevas-Diaz, V. Vazquez-Hipolito, Linear and nonlinear kinetic and isotherm adsorption models for arsenic removal by manganese ferrite nanoparticles, Sn Applied Sciences, 1 (2019) 1-19.

[61] O. Schabenberger, F.J. Pierce, Contemporary statistical models for the plant and soil sciences, CRC Press, Boca Raton, 2002.

[62] R.B. Darlington, Regression analysis and linear models : concepts, applications, and implementation, New York, New York; London : The Guilford Press, New York, 2017.

[63] M. Ferrante, B. Brunone, S. Meniconi, B.W. Karney, C. Massari, Leak size, detectability and test conditions in pressurized pipe systems, Water Resources Management, 28 (2014) 4583-4598.

[64] W. Nixon, M. Ghidaoui, A. Kolyshkin, Range of validity of the transient damping leakage detection method, Journal of Hydraulic Engineering, 132 (2006) 944-957.

[65] P.J. Lee, J.P. Vítkovský, M.F. Lambert, A.R. Simpson, J.A. Liggett, Leak location using the pattern of the frequency response diagram in pipelines: a numerical study, Journal of Sound Vibration, 284 (2005) 1051-1073.

[66] B. Brunone, M. Ferrante, M. Cacciamani, Decay of pressure and energy dissipation in laminar transient flow, Journal of Fluids Engineering, 126 (2004) 928-934.

[67] E. Kreyszig, Advanced Engineering Mathematics, 10th Eddition, Wiley, 2009.

[68] R.J. Sobey, Analytical solution of non-homogeneous wave equation, Coastal Engineering Journal, 44 (2002) 1-23.

[69] H.F. Duan, M.S. Ghidaoui, Y.K. Tung, Energy analysis of viscoelasticity effect in pipe fluid transients, Journal of Applied Mechanics-Transactions of the ASME, 77 (2010).

[70] H.F. Duan, T.C. Che, P.J. Lee, M.S. Ghidaoui, Influence of nonlinear turbulent friction on the system frequency response in transient pipe flow modelling and analysis, Journal of Hydraulic Research, 56 (2018) 451-463.

[71] H.F. Duan. Uncertainty analysis of transient flow modeling and transient-based leak detection in elastic water pipelines, Water Resources Management, 29(2015): 5413-5427.

[72] H.F. Duan (2016). Sensitivity analysis of transient based frequency domain method for extended blockage detection in water pipeline systems. Journal of Water Resources Planning and Management, 142(2016), 04015073.

[73] H.F. Duan. Accuracy and sensitivity evaluation of TFR method for leak detection in multiple-pipeline water supply systems. Water Resources Management, 32(2018), 2147-2164.